Redox Biology 50 (2022) 102229

Contents lists available at ScienceDirect

Redox Biology

journal homepage: www.elsevier.com/locate/redox

Cognitive enhancement and neuroprotective effects of OABL, a sesquiterpene lactone in 5xFAD Alzheimer's disease mice model

Jiang-Jiang Tang [a,*,1], Lan-Fang Huang [a,1], Jia-Le Deng [a], Yi-Meng Wang [a], Cong Guo [a], Xiao-Na Peng [a], Zhigang Liu [b,**], Jin-Ming Gao [a,***]

[a] Shaanxi Key Laboratory of Natural Products & Chemical Biology, College of Chemistry & Pharmacy, Northwest A&F University, Yangling, 712100, Shaanxi, PR China
[b] Laboratory of Functional Chemistry and Nutrition of Food, College of Food Science and Engineering, Northwest A&F University, Yangling, 712100, Shaanxi, PR China

ARTICLE INFO

Keywords:
Alzheimer's disease
Neuroprotection
Neuroinflammation
1,6-*O,O*-Diacetylbritannilactone (OABL)
Microglia
5xFAD mice

ABSTRACT

Alzheimer's disease (AD) is a neurodegenerative disease in which oxidative stress and neuroinflammation were demonstrated to be associated with neuronal loss and cognitive deficits. However, there are still no specific treatments that can prevent the progression of AD. In this study, a screening of anti-inflammatory hits from 4207 natural compounds of two different molecular libraries indicated 1,6-*O,O*-diacetylbritannilactone (OABL), a 1,10-*seco*-eudesmane sesquiterpene lactone isolated from the herb *Inula britannica* L., exhibited strong anti-inflammatory activity *in vitro* as well as favorable BBB penetration property. OABL reduced LPS-induced neuroinflammation in BV-2 microglial cells as assessed by effects on the levels of inflammatory mediators including NO, PGE_2, TNF-α, iNOS, and COX-2, as well as the translocation of NF-κB. Besides, OABL also exhibited pronounced neuroprotective effects against oxytosis and ferroptosis in the rat pheochromocytoma PC12 cell line. For *in vivo* research, OABL (20 mg/kg B.W., *i.p.*) for 21 d attenuated the impairments in cognitive function observed in 6-month-old 5xFAD mice, as assessed with the Morris water maze test. OABL restored neuronal damage and postsynaptic density protein 95 (PSD95) expression in the hippocampus. OABL also significantly reduced the accumulation of amyloid plaques, the Aβ expression, the phosphorylation of Tau protein, and the expression of BACE1 in AD mice brain. In addition, OABL attenuated the overactivation of microglia and astrocytes by suppressing the expressions of inflammatory cytokines, and increased glutathione (GSH) and reduced malondialdehyde (MDA) and super oxide dismutase (SOD) levels in the 5xFAD mice brain. In conclusion, these results highlight the beneficial effects of the natural product OABL as a novel treatment with potential application for drug discovery in AD due to its pharmacological profile.

1. Introduction

Alzheimer's disease (AD) is the most common underlying age-related dementia, and amyloid plaques (deposits of Aβ) and neurofibrillary tangles (hyperphosphorylated Tau) are the two major neuropathological hallmarks of AD [1]. The current therapeutic strategy for AD treatments is mainly single-target drugs via acting on β-amyloid (Aβ) or tau phosphorylation. However, numerous clinical trials were successively terminated [2]. An increasing number of studies have revealed that therapeutic strategies focused on targeting Aβ or tau phosphorylation can be insufficient due to the chronic and irreversible impairment of the nervous system in the late stage of AD [3–5]. Therefore, it is essential to seek more therapeutic-target drugs to modulate the AD microenvironment. Currently, multifunctional molecules capable of simultaneously interacting with several pathological components have been considered as a solution to increase the therapeutic index of AD.

Uncontrollable neuroinflammation and oxidative stress are important factors in the etiology and pathogenesis of AD [6]. Early AD is characterized by inflammatory responses and oxidative stress, which were reported to precede the appearance of the amyloid cascade. Inflammation is often accompanied by immune system activation, mediating primarily by glial cells, such as microglia and astrocytes [7].

* Corresponding author.
** Corresponding author.
*** Corresponding author.
E-mail addresses: tangjiang11@nwafu.edu.cn (J.-J. Tang), zhigangliu@nwsuaf.edu.cn (Z. Liu), jinminggao@nwafu.edu.cn (J.-M. Gao).
[1] The authors contributed equally.

https://doi.org/10.1016/j.redox.2022.102229
Received 17 December 2021; Received in revised form 30 December 2021; Accepted 5 January 2022
Available online 8 January 2022

Microglia are believed to control the balance of metabolism in the brain, including the secretion of proinflammatory such as NO, PGE_2, TNF-α, iNOS, and COX-2, or anti-inflammatory cytokines such as IL-10 and Arg-1. Additionally, conversion of microglia from proinflammatory profile to anti-inflammatory profile was associated with the inhibition of NF-κB signaling [8]. However, in the AD case, the balance is interrupted and excessively toxic agents can cause abnormalities in the AD microenvironment, which in turn leads to neuronal damage, aggravates the inflammatory responses, and accelerates AD progression [9]. Recent studies have found that by targeting microglia, many traditional medicines and natural products have shown great progress toward the prevention and treatment of AD [10–13].

In addition, oxidative stress has been shown in extensive studies to contribute significantly to the early onset and progression of AD [14,15]. ROS is a typical feature of oxidative stress and a key initiator of neuronal damage. Eliminating the oxidative stress cascade to correct the abnormal microenvironment has been proven as a new perspective, which has great potential for early AD treatment. For example, 7-*O*-Esters of taxifolin possessed pronounced neuroprotective effects against oxytosis, ferroptosis and ATP depletion [13]; curcumin could regulate the microglial inflammatory microenvironment [16,17]. Besides, many evidences have pointed out that activating the cellular antioxidant capacity is important to defend oxidative stress [18]. Although the removal of excess ROS has been confirmed as an effective means to normalize oxidative stress, regulating the function of damaged cells from a further upstream perspective is a new strategy that has significant potential for long-term treatment of AD. Antioxidants, as a first choice, have already been reported of possessing positive effects on AD models *in vitro* and *in vivo* [19–21]. However, these antioxidants therapies are still controversial in the use for AD patients due to their low penetration of blood-brain barrier (BBB) and poor bioavailability [21,22]. Thus, it is necessary to seek new alternatives for AD treatment.

Phenotypic screening continues to be more successful than target-based approaches for the discovery of first-in-class small molecule drugs [23,24]. Sesquiterpene lactones (STLs) are the main active ingredients of many medicinal plants from the Asteraceae family. Preparations from these plants are used in traditional medicine to treat inflammation [25]. For example, parthenolide, a renowned plant STL, was used extensively as a herbal remedy for treatment of multiple inflammatory diseases, including fever, migraine, arthritis, psoriasis, and atherosclerosis, with few mild side effects [26,27]. 1,6-*O,O*-diacetylbritannilactone (OABL) is another plant STL of 1,10-seco-eudesmanolide mainly extracted from *Inula britannica*. The genus Inula belongs to the family Asteraceae, which includes over 100 species distributed in temperate regions of Asia and Europe. Many *Inula* species have been used as traditional herbal medicines throughout the world for the treatment of bronchitis, diabetes, intestinal ulcers, digestive disorders, and inflammation [28]. For example, the dried flowers of *I. britannica* were officially listed in the Chinese Pharmacopoeia (2020 edition) for the treatment of bronchitis, digestive disorders, and inflammation. As a main active ingredient of this plant, OABL also could suppress NO and PGE_2 synthesis in RAW264.7 macrophages [29], and antitumor activities [30]. In addition, ABL, an analog of OABL, has been reported to possess the ability of inhibiting COX-2 and NF-κB expression and further improving learning and memory in $A\beta_{23\text{-}35}$-induced rats [31]. Nevertheless, the mechanisms by which ABL or OABL may ameliorate AD remain elusive. Considering the multifactorial pathogenesis of AD, multi-targets have become a focus in the discovery of drugs from natural products with anti-inflammatory and antioxidant features. In this study, a phenotypic-based screening from 4207 compounds library was performed against neuroinflammation, and OABL was found as a new hit with pronounced effects in anti-neuroinflammation and neuroprotection as well as good BBB penetration. Furthermore, we explored the effect of OABL in 5xFAD mice, a recognized transgenic mouse model of AD, by investigating the biological mechanisms underlying its potential therapeutic effect.

2. Materials and methods

2.1. Compounds library, and ABL and OABL isolation

Two compounds libraries were used in the initial screening of biological activity. One is a lab in-house compounds library of 1407 molecules, which has been constructed in Nov 2018, including 1209 natural products and 198 synthetic compounds. The other is the natural products library of 2800 molecules obtained from TargetMol Co. (Boston, MA, USA). Natural products ABL and OABL were obtained from the air-dried flowers of *I. britannica* by repeated silica gel column chromatography and preparative TLC with >98% HPLC purity [30,32].

2.2. Nitric oxide production inhibitory screening assays in BV-2 cells

Murine microglial BV-2 cells were obtained from Peking Union Medical College Cell Bank (Beijing, China). Briefly, BV-2 cells (2×10^4/well) were seeded in 96-well plates and incubated at 37 °C for 24 h before compounds treatment for 24 h in the presence of 1 μg/mL LPS (*Escherichia coli* 0111: B4, Sigma, U.S.). The NO concentration (nitrite) in the medium was tested by a micro NO content assay kit (Solarbio, China). After adding Griess reagents, the absorbance at 540 nm was measured by a microplate reader. EC_{50} values were calculated as the concentrations of reducing 50% NO production. Meanwhile, the cytotoxicity (CC_{50}) of compounds was evaluated by the MTT assay refer to our previous report [33].

2.3. Immunofluorescence for NF-κB translocation assay in BV-2 cells

BV-2 cells were seeded in Eppendorf Cell Imaging 8-well coverglasses for 24 h, and the cells were pretreated with OABL with various concentrations for 1 h and then activated by LPS (1 μg/mL) for 24 h. Afterward, the cells on coverglasses were washed and fixed with cold 4% paraformaldehyde (PFD), and permeabilized with 0.2% Triton X-100 (in PBS). Then, the cells were blocked with 5% bovine serum albumin (BSA in PBS) for 1 h, and incubated overnight at 4 °C with primary antibody anti–NF–κB p65 (rabbit monoclonal IgG, 1:100 dilution). After removing the primary antibody, the cells were washed with PBS and incubated with anti-rabbit IgG (H+L), F(ab')2 Fragment (Alexa Fluor® 647 Conjugate) (1:500–1:2000 dilution) for 1 h. Finally, the cells were counterstained with 4′,6-diamidino-2-phenylindole (DAPI) for 10 min. Removing the chamber by lifting it upwards, and images were taken using a confocal fluorescence microscope (Leica).

2.4. Cell viability assay in PC12 cells

Rat pheochromocytoma PC12 cell line was purchased from the Shanghai Institute of Biochemistry and Cell Biology (Chinese Academy of Sciences). PC12 cells cultured in PLL-coated 96-well plates were incubated with OABL or OABL-GSH in fresh medium containing 2% horse serum (HS) and 1% FBS for 24 h at 37 °C. After replacement with fresh medium containing 0.6 mM H_2O_2, 1.0 mM 6-OHDA, 100 mM glutamate (Santa Cruz Biotechnology, U.S.) or 10 μM RSL3 (Sigma, U.S.) for 24 h, MTT (Solarbio, China) was added and incubated for another 4 h. After the solubilization of purple formazan in DMSO, the optical density of absorbance was measured at 490 nm.

2.5. Michael acceptor assay by HPLC-MS and synthesis of OABL-GSH

OABL (1 mM) solution of PBS:DMSO (4:1, pH = 7.2) at 37 °C was added the reduced glutathione (GSH, 5 mM). The HPLC-MS with 254 nm and 190 nm UV detectors was recorded at different time points. HR-ESIMS (AB Sciex, U.S.) was detected the peak of OABL-GSH adduct.

Synthesis of OABL-GSH: to a solution of OABL (9.0 mg, 1 eq.) in 1.5 mL of MeOH was added a solution of GSH (19 mg, 2 eq.) and Et_3N (10 μL, 2 eq.) in 0.5 mL of H_2O. The mixture was stirred for 1.0 h at room

temperature, and then target compound was obtained by the preparative HPLC (10–100% MeOH in water). OABL-GSH: HR-ESIMS (*m/z*): calculated for $C_{29}H_{43}N_3O_{12}S$ $[M + H]^+$ 658.2640, found: 658.2644.

2.6. Detection of reduced glutathione (GSH) in live cells

PC12 cells were added to the 96-well black-flat plates (Costar) and allowed to attach for 24 h. For 2 h or 24 h treatment group, the medium was removed out, and cells were washed with free-FBS medium 3 times and 90 μL fresh free-FBS medium was added and then 10 μL various concentrations of OABL. After that, reduced GSH level in live cells was detected by cellular GSH detection assay kit (No.13859, Cell Signaling, U.S.). 10 μL of live cell staining working solution was added to each well containing 100 μL of growth media, and cells were incubated for 30 min. For best results, measure the fluorescence intensity every 30 min for up to 3 h or until the signal has reached a plateau. The fluorescent intensity was measured at an excitation wavelength of 380 nm and an emission wavelength of 460 nm using a SpectraMax M5 plate reader (Molecular Devices, U.S.).

2.7. Permeability assay in vitro

The ability to penetrate the blood−brain barrier (BBB) was evaluated by the parallel artificial membrane permeation assay (PAMPA) refer to the previous method [34,35].

2.8. Acetylcholinesterase inhibitory activity

The modified Ellman's method for a 96-well plate was used to assay the activity of compounds against acetylcholinesterase (AChE) (Sigma). Acetylcholinesterase iodide (ATCI) (Aladdin) as a substrate was prepared in PBS (0.1 M, pH = 7.4) with the concentration of 7.5 mM. The experimental solution of AChE was obtained by diluting 50 U/mL sample of AChE to 1.5 U/mL with PBS (0.1 M pH = 7.4) and Ellman's reagent 5,5' -dithio-bis(2-nitrobenzoic acid) (DTNB) (Sigma) was diluted by PBS (0.1 M, pH = 7.4) to 10 mM. Stock samples (20 mM) were prepared in dimethyl sulfoxide (DMSO) and appropriately diluted in PBS (0.1 M pH = 7.4). All experiments were blank control group (neither AChE nor samples), negative control group (only AChE), experimental group (AChE and samples). Galantamine was used as a positive control. Firstly, PBS was added respectively to blank control, negative control, and experimental groups. Except for blank control group, others were added 20 μL of 1.5 U/mL AChE. Then, 20 μL of 200 μM compounds including were added into experimental wells. Next, each well was added 60 μL of 10 mM DTNB. The plate was placed on crushed ice and cooled for 20 min. After that, the mixture was read once a minute for 40 min at 37 °C with a microplate reader.

2.9. Animals and OABL administration

On a congenic C57BL6 background, the male transgenic mice with 5xFAD mutations (Stock No: 006554) were obtained from the Jackson Laboratory (Bar Harbor, ME, USA) and maintained periodically backcrossed with female C57BL6 stock (Stock No: 006554) from Jackson Labs. It is carried that human amyloid precursor protein (APP) and the human presenilin 1 (PSEN1) transgenes with a total of five AD-associated mutations in 5xFAD mice, which includes the Swedish (K670 N/M671L), Florida (I716V), and London (V717I) mutations in APP, and the M146L and L286V mutations in PSEN1. In order to recognize the genotype of future generations, mice were tested for both the APP and PS1 genes with polymerase chain reaction (PCR). DNA samples were gained from ear tissue (DNA extraction Kit (centrifugal column), Beijing Betek Biotechnology Co. Ltd). Besides, mice had the $Pde6b^{rd1}$ allele, a recessive mutant gene, which leads to retinal dysfunction. To prevent the interference of visual impairment, the $Pde6b^{rd1}$ allele-carried mice were excluded from the study. In this study, the 5xFAD mice were used to perform animal experiments while age-matched mice on the same background were used as the controls. All animals were housed in the facility of Northwest A&F University under standard conditions (12/12 light-dark cycles, temperature 22 ± 2 °C, humidity at 50 ± 15%). Furthermore, experimental mice were separated as one per cage. Meanwhile, a standard diet including pure water and AIN-93 M (TROPHIC Animal Feed High-Tech Co., Ltd) were given to all animals. After experimental mice were fed for 6 months, the 5xFAD and wild-type (WT) mice were freely assigned to 4 groups based on genotypes (n = 8/group): WT+Vehicle, WT+OABL, 5xFAD+Vehicle, 5xFAD+OABL.

OABL (20 mg/kg per day) dissolved in water with 10% ethanol and 10% Tween 80 was administrated to 6-month-old WT and 5xFAD mice for 3 weeks. WT+OABL and 5xFAD+OABL groups were treated by an intraperitoneal (*i.p.*) injection of OABL as the above-mentioned. OABL were dissolved in 10% ethanol, 10% Tween 80 and distilled water (according to 0.1% w/vol), and this solution of 10% ethanol, 10% Tween 80, and 80% distilled water was used as the vehicle. Mice from WT+Vehicle group and 5xFAD+Vehicle group were injected with the vehicle. Additional animal tests were conducted after *i.p.* injection. All of the experimental procedures with animals were carried out following the Guide for the Care and Use of Laboratory Animals (Eight Edition, ISBN-10:0–309-15396-4), and the animal protocol was approved by the animal ethic committee of Northwest A&F University (N81803231).

2.10. Morris water-maze test

The Morris water maze is one of the most widely used tests in behavioral neuroscience for studying the psychological processes and neural mechanisms of spatial learning and memory. The protocol was detailed described as following: the apparatus consists of a large circular pool with a diameter of 1.5 m and a height of 35 cm (XR-XM101, Shanghai Xinruan Information Technology Co. Ltd), containing water at around 25 °C. The mice received four habituation training on day 0. The platform was visible (2 cm above the water surface), and the water was undyed. Test trials were conducted for 5 consecutive days (day 1−day 5). All the data were recorded automatically via a video tracking system (SuperMaze software, Shanghai Xinruan Information Technology Co., Ltd).

2.11. Tissue processing

The brain was removed as cerebellum and brain stalk, and other tissues were also collected. The tissues were then placed in a vial with 4% paraformaldehyde in PBS (pH 7.4) for 24 h at room temperature (n ≥ 3, for H&E and immunochemical staining) or frozen (n ≥ 5, for other biochemical examination) until analysis. The prepared tissues were fixed for more than 24 h before being dehydrated with gradient alcohol. The samples were sequentially soaked in alcohol-benzene and xylene, and then embedded in paraffin. The wax-soaked tissues were cut into slices of a thickness of 4 μm. Finally, the finished pieces were stored at room temperature.

2.12. Hematoxylin and eosin (H&E)

The wax pieces of tissues of the brain, heart, liver, spleen, lung, and kidney were prepared. In the beginning, different sections were dewaxed using xylene (twice, 20 min each time) and gradient ethanol (100%, twice, 5 min; 75%, once, 5 min). After being washed in water, wax slices were stained with hematoxylin and eosin. Finally, entire pieces were undertaken using an optical microscope (Olympus).

2.13. Immunohistochemical staining

Fixed brain sections were immersed in xylene and gradient ethanol for deparaffinization and rehydration. Afterward, the brain pieces were

placed in citric acid (pH 6.0) antigen retrieval buffer for antigen retrieval and in PBS (pH 7.4) and shaken on the decolorization shaker 3 times for 5 min each. For the purpose of blocking endogenous peroxidase activity, the slices were put into 3% hydrogen peroxide and incubated at room temperature in darkness for 25 min. Then, the same operation was performed in PBS as before. 3% BSA was added to the circle to evenly cover the tissue, and the tissues were sealed for 30 min at room temperature (primary antibody was sealed with normal rabbit serum from goat source, and other sources were sealed with BSA). The primary antibody incubated sections at 4 °C overnight, including GFAP (Servicebio, China), $A\beta_{1\text{-}42}$ (Proteintech, U.S.), Iba-1 (Servicebio). The sections were washed by PBS before being incubated with the corresponding secondary antibody at room temperature for 50 min. The same washing step was repeated using PBS, and the 3, 3′-diaminobenzidine tetrahydrochloride (DAB) was then utilized for dyeing prepared samples. Next, hematoxylin was used to re-dye, and neutral resin was use to block the brain slices. In the end, the acquisition of images from stained sections was employed by the optical microscope (Olympus). For thioflavin-S staining, the brain sections were placed in 1% aqueous thioflavin-S for 8 min, then washed in distilled water, and dehydrated through 70%, 90%, and 100% ethanol for 1 min in each grade. The sections were then mounted in a mounting medium (Solarbio). The representative images were captured from the hippocampus and cortex.

2.14. Immunofluorescence labeling

As previously described, the procedure of immunofluorescence staining is similar to immunohistochemistry. After dewaxing, the sections were placed in EDTA antigen buffer for antigen recovery and washed by PBS for 5 min × 3. 3% BSA (for the case of primary antibody originated from others) was used to cover the marked tissues to block non-specific binding for 30 min, while 10% donkey serum covered objective area (for the case of primary antibody originated from goat). Then, the slices were incubated with primary antibodies likes GFAP, $A\beta_{1\text{-}42}$, Iba-1 overnight at 4 °C. After PBS washing, the sections were incubated using a secondary antibody (FITC, CY3, Alexa Fluor® Plus 647, Invitrogen) at room temperature for 50 min in dark conditions. Histologic pieces were further incubated with DAPI under the same conditions as in the stage of secondary antibody. Last but not least is the case that brain sections were washed in PBS, added spontaneous fluorescence quenching reagent for 5 min, and sealed with anti-fade mounting medium. Microscopy detection and images were collected by fluorescent microscopy (Olympus). DAPI glows blue; FITC glows green; CY3 glows red; Alexa Fluor® Plus 647 glows pink. The positive region was quantified by ImageJ software.

2.15. qRT-PCR analysis

Total RNA from frozen brain tissues was extracted with AG RNAex Pro reagent (Accurate Biotechnology Co.) according to the manufacturer's instructions. For real-time PCR, the sample was reversed transcribed into cDNA with Evo M-MLV RT kit (Accurate Biotechnology Co.) following determination of the concentration of obtained RNA with Micronucleic acid quantifier (NanoDrop 2000/2000c UV–Vis, Thermo Fisher Scientific). Relative mRNA expression was qualified using SYBR Green Premix Pro Taq HS qPCR kit (Accurate Biotechnology Co.) and specific primers. Then, quantitative PCR was carried out using Real-Time PCR Systems (QuantStudio™ 6 Flex, Thermo Fisher Scientific), and GAPDH was considered as an endogenous control. All reactions were performed in triplicate in 0.1 mL 8-tube strips. The procedure was as followed: 95 °C for 10 min, then 95 °C for 15 s, and 60 °C for 1 min in 40 cycles. To analyze the relative changes in gene expression, the $2^{-\Delta\Delta CT}$ method was adopted. Reagent information and primers sequence were shown below (Table 1).

Table 1
List of primers and primer sequences.

	forward primer (5'-3')	reverse primer (5'-3')
BACE-1	CCGGCGGGAGTGGTATTATGAAGT	GATGGTGATGCGGAAGGACTGATT
TNF-α	CCCTCACACTCAGATCATCTTCT	GCTACGACGTGGGCTACAG
IL-1β	TGACGGACCCCAAAAGAHTGA	TCTCCXACAGCCACAATGAGT
GAPDH	TGGAGAAACCTGCCAAGTATGA	TGGAAGAATGGGAGTTGCTGT

2.16. Western blotting

In vitro. BV-2 cells were stimulated with or without 1 μg/mL LPS and treated with DMSO or OABL of different concentrations. After treatment for 24 h, dish cells were gently scratched off. Precool lysis buffer containing 25 mL HEPES, 2.5 mg catalase (Bimake), 0.25 mL IGEPAL (Solarbio) wad added to the pelleted cells. After centrifuge at 14,000 g for 20 min at 4 °C, samples protein concentrations were quantified by the method of a bicinchoninic acid (BCA) assay kit (TIANGEN, China). Equal amounts of protein were run on 4%–20% sodium dodecyl sulfate-polyacrylamide gels (SDS-PAGE) (Beyotime, China) and transferred to nitrocellulose filter (NC) membranes (Millipore, U.S.). The membranes were blocked by 5% nonfat milk (BD) in TBST (20 mM Tris–HCl, pH 7.6, 150 mM NaCl, and 0.1% Tween-20) for 1 h, and was incubated with the desired primary antibody diluted in 5% BSA (Solarbio) in TBST at 4 °C overnight. After being washed, the membrane was incubated with the specific secondary antibody diluted in 5% non-fat milk in TBST for 2 h. The immunoreactive bands were visualized by the Chemiluminescence Western Blotting Detection system (Thermo Fisher Scientific, U.S.). Main primary antibodies: rabbit monoclonal anti-iNOS (1:1,000, Abcam, U.S.), rabbit monoclonal anti-COX-2 (1:1,000, CST, U.S.), mouse monoclonal anti–NF–κB p65 (1:1000, Santa Cruz, U.S.), rabbit monoclonal anti-Lamin B1 (1:1000, abways, China), rabbit monoclonal anti-β-Tubulin (1:1,000, Proteintech, U.S.). Secondary HRP-conjugated antibodies used were goat anti-mouse IgG (1:5,000, SAB, U.S.) and goat anti-rabbit IgG (1:5,000, SAB).

In vivo. The protein of brain tissues was extracted using a protein-extraction reagent. A BCA kit was used to quantify the samples. The total tissue proteins (n = 6) were separated by SDS-PAGE, and then transferred onto a NC membrane by using a wet transfer apparatus. Then membranes were incubated in 5% skim milk for 1 h at room temperature. Next, the blots were incubated overnight at 4 °C with primary antibodies. The membranes were incubated with anti-rabbit HRP-conjugated secondary antibody (1:5,000, SAB) for 1 h at room temperature. The bands were visualized with enhanced chemiluminescence and exposed on an Imager Chemidoc XRS System (Bio-Rad). Main primary antibodies: rabbit monoclonal anti-BACE1 (1:1,000, CST), rabbit monoclonal anti-GFAP (1:1,000, CST), rabbit monoclonal anti-Iba1 (1:1,000, CST).

2.17. Electron microscopy for structural analysis of the hippocampus

The hippocampus was split and treated in a cold fixative solution made up of 2.5% glutaraldehyde (pH 7.2) at 4 °C for 4 h. They were then washed with PBS (0.1 mol/L, pH 7.2) thrice. Then the specimens were post fixed in 1% OsO_4 (in 0.2 mol/L PBS, pH 7.2) at 4 °C for 1 h and washed again with PBS (0.1 mol/L, pH 7.2) thrice. The specimens were dehydrated for 15–20 min each in a graded series of ethanol solutions (30, 50, 70, 80, 90, and 100%) and then transferred to acetone for 20 min incubation. Materials were then permeated in an acetone−resin mixture (1:1) for 1 h at 25 °C and then transferred to an acetone−resin mixture (1:3) overnight. Ultrathin sections were placed in the region which was closed to the embedded blocks and kept away from the dorsal rim area, stained with uranyl acetate and alkaline lead citrate for 15 min, and then observed using a transmission electron microscope (TEM, HT7800, HITACHI, Japan).

2.18. ELISA assay

In vitro. The levels of cytokines PGE_2 and TNF-α were determined by ELISA. In brief, BV-2 cells were seeded in 96-well plates and incubated at 37 °C for 24 h. The cells were activated by LPS (1 μg/mL) and treated with OABL (1, 2.5, 5, and 10 μM) for another 24 h. The culture medium was collected and centrifuged at 12,000 rpm for 10 min. The level of TNF-α and PGE_2 in the culture medium was quantified using mouse ELISA kits (R&D Systems, U.S.).

In vivo. The brain tissues were rinsed with PBS, cut into 1–2 mm pieces, and homogenized with a tissue homogenizer in PBS. An equal volume of tissue protein extraction reagent (Thermo, U.S.) containing protease inhibitors was added and tissues were lysed on ice for 30 min with gentle agitation. Debris was then removed by centrifugation. Aliquots of the lysates were removed and amyloid β concentrations in tissue lysates were determined according to the Human Amyloid β (aa1-42) ELISA Kit (R&D Systems, U.S.). For the levels of p-Tau protein, cortex pieces were weighed and then minced to small pieces which will be homogenized in PBS (mass ratio of 1:10). The homogenates were then centrifugated to get the supernate. Blood supernatant was obtained by centrifugation after blood was taken from mouse orbit, and stored at −80 °C. Then the levels of p-Tau protein in the cortex and serum were determined by the Mouse phosphorylated Tau protein ELISA kit (MLBio).

2.19. Oxidative stress assay

The cortex of mice brain was rinsed with PBS, cut into 1–2 mm pieces, and homogenized with a tissue homogenizer in PBS (mass ratio of 1:10). The homogenates were centrifuged at 3000 r/min for 10 min at 4 °C and the supernatants were collected. Total GSH in cortex was assayed using the 5,5-dithio-bis (2-nitrobenzoic) acid (DTNB) method according to the manufacturer's protocols (Cat NO: BC1170, Solarbio). The T-SOD activity was determined according to Total Superoxide Dismutase (T-SOD) assay kit (Hydroxylamine method, Cat NO: A001-1-2) from Nanjing Jiancheng Bioengineering Institute. MDA level was determined by homogenizing the cortex in PBS with EDTA and then according to Malondialdehyde (MDA) assay kit (TBA method, Cat NO: A003-1-2) from Nanjing Jiancheng Bioengineering Institute.

2.20. Statistical analysis

Statistical analysis was applied by student's t-test or two-way analysis of variance (ANOVA) followed by Newman-Keuls multiple comparison test using GraphPad Prism 8.0. Details of the statistical analyses applied to each data set, the number of subjects, and the resulting *p* values are described in the figure legends. All results were presented as mean ± SEM for each group.

3. Results

3.1. Phenotypic screening of anti-neuroinflammation hits in LPS-induced BV-2 microglial cells

Augmented NO combines with ROS to generate the highly toxic peroxynitrite ($ONOO^-$), which easily crosses cellular membranes and induces neuronal damage [36]. Using LPS-induced BV-2 cells model, 4207 compounds, including 1407 compounds from our lab in-house small molecules library and 2800 of natural compounds library for HTS from TargetMol (https://www.targetmol.com/compound-library) were screened against LPS-induced BV-2 cells. Given the cytotoxicity, we simply screened out the 102 compounds with potential activity (inhibition rate at 10 μM: > 80%) and low cytotoxicity (< 10%, Fig. S1A). Further *in silico* analysis of druggability containing molecular weights (MW, ≤ 400), clog P (≤5), total polar surface area (tPSA, ≤ 90 $Å^2$), absorption, distribution, metabolism, excretion, and toxicity (ADMET) properties, and 9 compounds were selected. Among them, two natural analogs 1-*O*-acetylbritannilactone (ABL) and 1,6-*O*,*O*-diacetylbritannilactone (OABL) have attracted our attention due to their potential NO inhibition effect with EC_{50} values of 12.5 μM and 6.3 μM, respectively (Fig. 1A and Fig. S1B) and low reduction in cell survival (less than 5%) at 20 μM [35]. Notably, ABL and OABL both showed sound blood-brain barrier (BBB) penetration capacity ($P_e = 7.5 \times 10^{-6}$ cm/s for ABL and 12.3×10^{-6} cm/s for OABL), which is essential for the effectiveness of CNS drugs (Fig. 1A and Table S1). Besides, OABL also exhibited *in silico* MW (350.41), clog P (2.69), tPSA (78.9 $Å^2$), and good ADMET properties. Due to the optimal physicochemical properties, OABL would be selected to perform more studies on *in vitro* and *in vivo* models. ABL and OABL were 1,10-*seco*-eudesmane sesquiterpene lactones, which were found at sufficient levels (~2%) in the traditional Chinese medicinal herb *Inula britannica* Linn. Besides, OABL can be easily and stoichiometrically obtained from the C-6 transformation of ABL.

Tumor necrosis factor-*α* (TNF-*α*) and prostaglandin E_2 (PGE_2) are two major inflammatory mediators of activated (M1) macrophages, and OABL significantly inhibited TNF-α and PGE_2 productions against LPS-induced BV-2 cells in a dose-dependent manner (Fig. 1B and C). The alternatively activated (M2) macrophages are beneficial in blocking inflammatory responses by producing high levels of anti-inflammatory cytokines, such as IL-10 and Arg-1. To characterize the effect of OABL in the polarization of BV-2 microglial cells, the M2 markers arginase-1 (Arg-1) and IL-10 were measured. As shown in Fig. 1D and E, IL-10 and Arg-1 levels were not markedly changed after LPS stimulation. Interestingly, OABL significantly increased the production of IL-10 at 10 μM but not enhanced the activity of Arg-1 at this concentration, indicating that OABL might partly promote the conversion of the microglia from M1 to M2 phenotype. OABL dose-dependently reduced the protein expression of iNOS and COX-2, which are the enzymes responsible for NO production and PGE_2 production, respectively (Fig. 1F and G). The NF-κB translocation is the main driver for the production of LPS-induced inflammatory mediators [37]. OABL could inhibit IκB kinase β-dependent NF-κB activation in LPS/IFN-γ-induced RAW264.7 macrophages [38]. Furthermore, the immunofluorescence staining and Western blotting experiments showed that OABL also blocked the translocation of NF-κB by adjusting the distribution of p65 in both the nucleus and cytoplasm in LPS-stimulated BV-2 cells (Fig. 1H–J). These results indicated that OABL exhibited potent anti-inflammatory properties via suppressing of the NF-κB signaling pathway and the microglia conversion from M1 to M2 phenotype, with favorable BBB penetration property and low cytotoxicity.

3.2. Protective effects of OABL on neuronal viability

GSH contains a mercapto moiety (-SH), which has the potential to react with the α,β-unsaturated carbonyl moiety of OABL. In order to determine the reactivity window of OABL, incubation of OABL and GSH in a solution of PBS: DMSO (4:1) at 37 °C quickly yielded an OABL-GSH adduct (HRMS: *m/z* 658.2644 $[M+H]^+$) in 90% transformation of OABL within 2 h detected at 254 nm UV detector by HPLC-MS in Fig. 2A and Fig. S2A. The recovery of OABL after 2 h remained less than 10% by analysis of the relative area of HPLC peaks (Fig. S2B), which showed the high reactivity of the α-methylene-γ-lactone motif of OABL by undergoing a Michael addition of the mercapto moiety of GSH in ^1H NMR spectra analysis (Fig. S2C). In our previous results, similar structures with α-methylene-γ-lactone motif can rapidly react with β-mercaptoethanol in DMSO [39]. It was noted that OABL is stable in PBS for up to 7 days.

Cellular GSH depletion results in ROS accumulation and cell death. To evaluate the effect of OABL on intracellular GSH levels within effective concentrations, the GSH level in live cells was detected for 2 h and 24 h with the treatment of OABL. OABL with < 20 μM showed no significant inhibition of cellular GSH level and cell proliferation at both

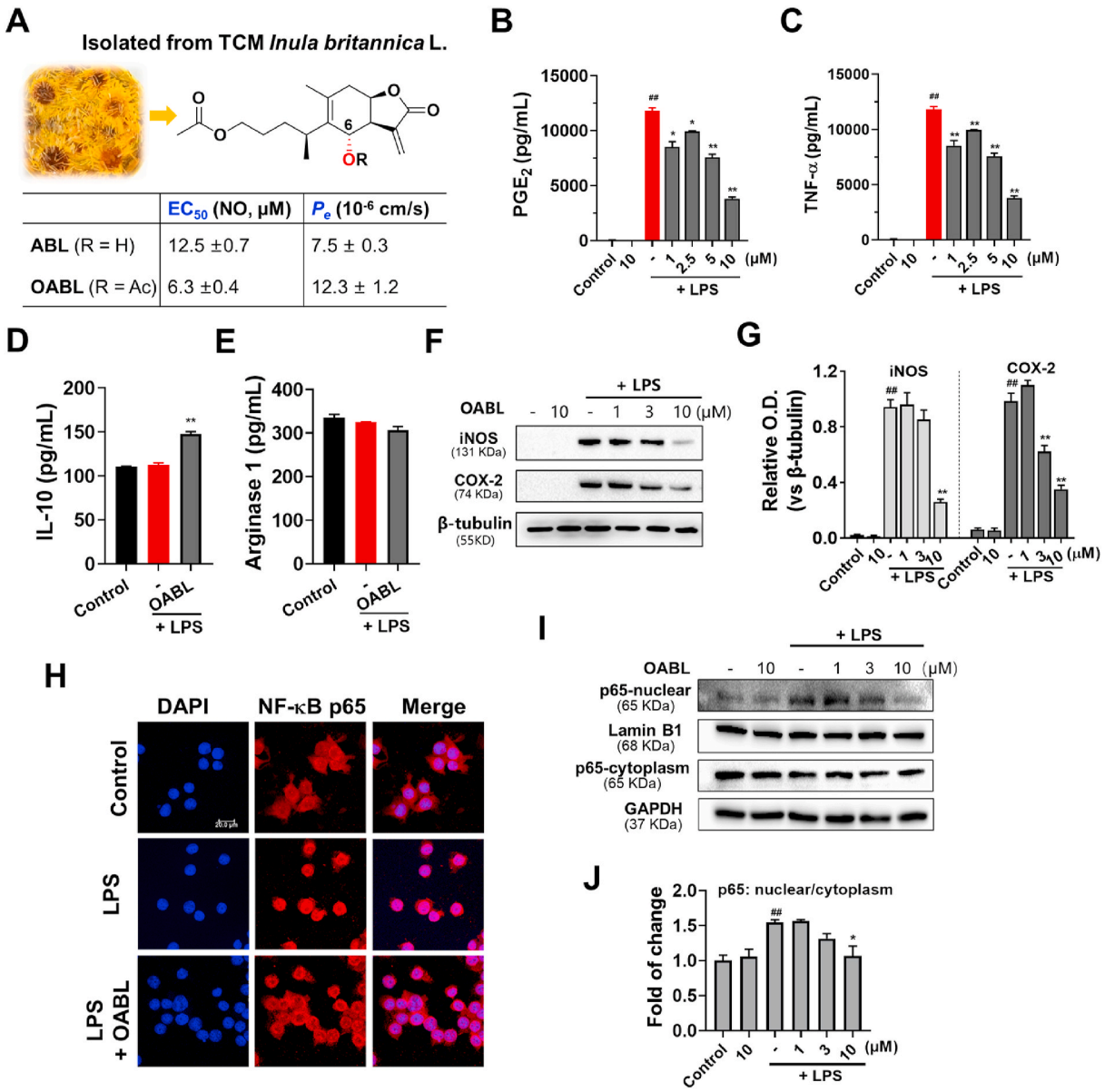

	EC_{50} (NO, μM)	P_e (10^{-6} cm/s)
ABL (R = H)	12.5 ±0.7	7.5 ± 0.3
OABL (R = Ac)	6.3 ±0.4	12.3 ± 1.2

Fig. 1. The preventive effects of OABL on neuroinflammatory responses in LPS-stimulated BV-2 microglial cells
(A) Chemical structures of natural products ABL and OABL, and their EC_{50} against NO production in LPS-stimulated BV-2 microglial cells and blood-brain barrier permeability (P_e); inhibition effects of OABL on PGE_2 production **(B)** and TNF-α **(C)** in LPS-stimulated BV-2 cells; **(D)** effect of OABL at 10 μM on IL-10 production; **(E)** Arginase 1 (Arg-1) effect of OABL at 10 μM. The TNF-α, PGE_2, IL-10 and Arg-1 levels in culture supernatant were determined by ELISA kit (R&D); **(F)** representative images of iNOS and COX-2 protein expression changes of OABL-treated BV-2 cells; **(G)** densitometric analyses of the iNOS and COX-2; **(H)** representative images of NF-κB p65 translocation of OABL at 10 μM. Immunofluorescence staining in both nucleus and cytoplasm by some colocalization of receptors (p65, red, Alexa Fluor 647) with nuclei (DAPI, blue) detected the distribution of NF-κB p65. Images were captured by confocal fluorescence microscope with 40 × objective, and the scale bar is 20 μm; **(I)** representative images of NF-κB p65 in the nucleus and cytoplasm in OABL-treated BV-2 cells; **(J)** densitometric analyses of the NF-κB p65 nuclear/cytoplasm. For these experiments, BV-2 cells were stimulated with or without 1 μg/mL LPS and treated with increasing concentrations of OABL for 24 h. The statistical analysis was performed by student's t-test, and all values are the mean ± SEM of three independent experiments. (##) $p < 0.01$ significantly different from the DMSO group; (*) $p < 0.05$ and (**) $p < 0.01$, *vs.* the LPS-treated control group. (For interpretation of the references to color in this figure legend, the reader is referred to the Web version of this article.)

time points of treatment, although GSH depletion occurred at higher concentrations of 50 μM and 100 μM due to cytotoxicity at the high concentration tested (Fig. 2B). Furthermore, the cytotoxic effect of OABL on PC12 cells was assessed. It was observed that treatment with OABL (0–20 μM) for 24 h did not indicate any cytotoxic effect on PC12 cell viability, thus indicating that OABL was not toxic to PC12 cells at the highest concentration used for this study (Fig. 2C).

Oxidative stress can induce neuronal damage implicated in neurodegenerative diseases [40]. The rat pheochromocytoma PC12 cell line is one of the most commonly used in neuroscience research [41]. H_2O_2 and 6-OHDA were used as oxidative stress inducers to evaluate the neuroprotection of OABL against oxidative damage. The cell viability of PC12 cells exposed to 0.6 mM H_2O_2 and 1.0 mM 6-OHDA for 24 h were decreased to 42.9% and 39.9% of controls, respectively. As the results shown in Fig. 2D and E, OABL was capable of rescuing the cell injury observed at all concentrations. In the H_2O_2-induced PC12 cells, pretreatment with different concentrations of OABL (1, 5, 10 μM) significantly recovered the cell viability to 45.9%, 57.8%, and 73.8% (Fig. 2D). Moreover, in the 6-OHDA-induced PC12 cells, the pretreatment with OABL (1, 5, 10 μM) was restored to 46.4%, 68.0%, and 61.9% (Fig. 2E).

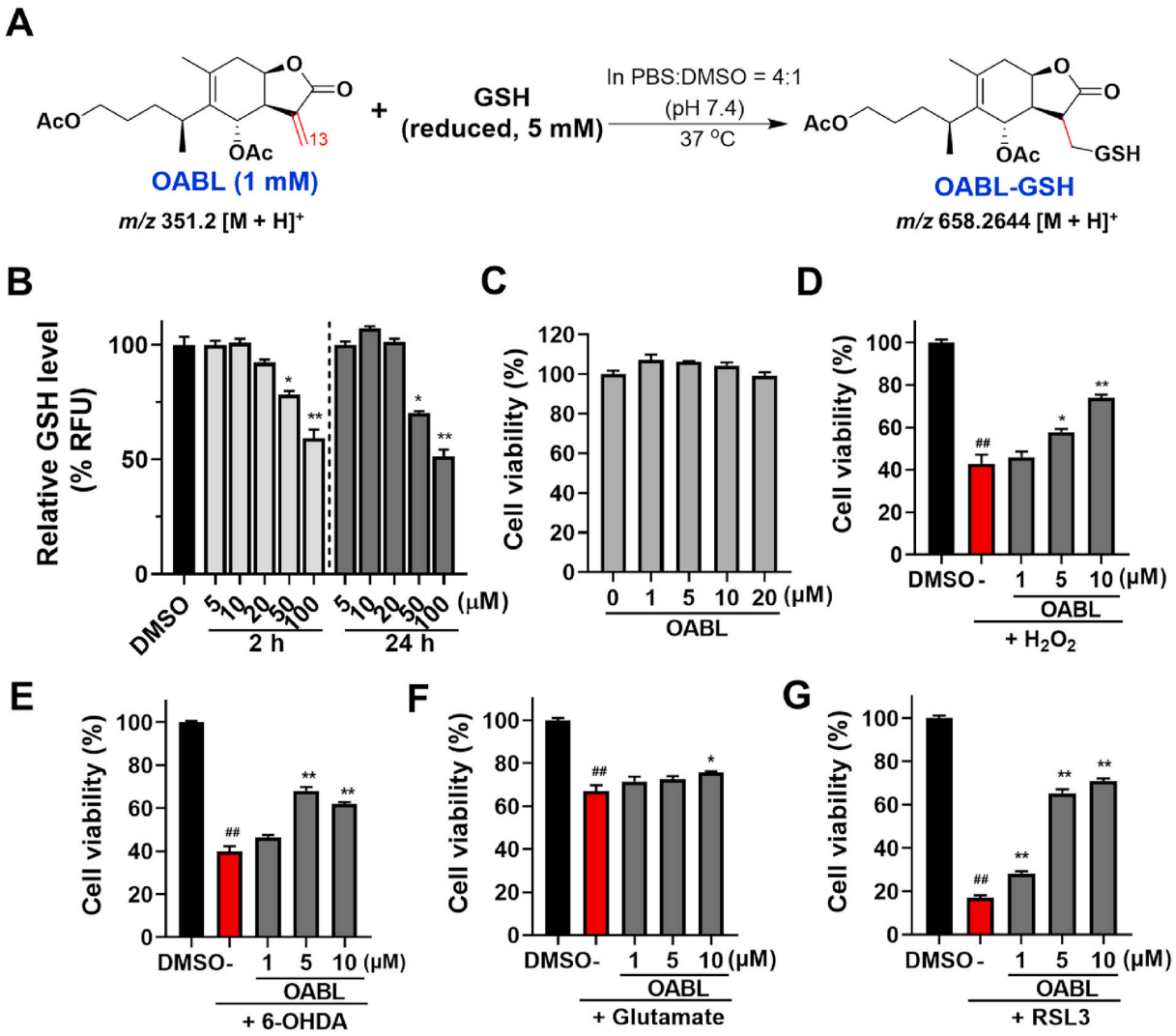

Fig. 2. The preventive effects of OABL on oxidative stress-induced PC12 neuronal death

(A) Reaction of OABL and GSH in PBS. OABL (1 mM) and GSH (5 mM) were incubated in a solution of PBS: DMSO = 4: 1 at 37 °C for 2 h, and the reaction progress was monitored by HPLC-MS (see Fig. S2 in Supplementary data); **(B)** detection of GSH in live cells. PC12 cells were treated by various concentrations of OABL for 2 h or 24 h. The GSH level was measured according to a cellular GSH detection assay kit (#13859, CST) with the fluorescent intensity at an excitation wavelength of 380 nm and an emission wavelength of 460 nm using a SpectraMax M5 plate reader; **(C)** neurotoxic effect of OABL against PC12 cells. Cells were incubated with vehicle and OABL (1, 5, 10, and 20 μM) for 24 h; **(D–G)** oxidative damage was induced by H_2O_2, 6-OHDA, oxytosis was induced by glutamate, and ferroptosis was induced with RSL3 in PC12 cells. PC12 cells were incubated with vehicle (0.1%, DMSO) and OABL (1, 5, and 10 μM) for 24 h, and then exposed to various inducers for 24 h. The cell viability was assessed by MTT assay; inhibition effects of OABL **(D)** in 0.6 mM H_2O_2-induced PC12 cells; **(E)** in 1.0 mM 6-OHDA-induced PC12 cells; **(F)** in 100 mM glutamate-induced PC12 cells; **(G)** in 10 μM RSL3-induced PC12 cells. The statistical analysis was performed via student's t-test, and the data are presented as the means ± SEM from three or five independent experiments, each with 4–6 duplicates. (##) $p < 0.01$ as compared to control (DMSO); (*) $p < 0.05$ and (**) $p < 0.01$ *vs.* the inducers-treated group.

However, the adduct OABL-GSH at the 5–20 μM had no influence on the H_2O_2-induced PC12 cells damage (Fig. S2D), which was similar to that derivatives with reduction or adduction of α-methylene motifs of OABL losing the effective activity of anti-neuroinflammation [35].

Glutamate treatment of PC12 cells leads to intracellular glutathione (GSH) depletion resulting in oxytosis, which is a form of programmed cell death due to oxidative stress. Oxytosis is induced by glutamate inhibiting cystine import by blocking system x_c^-. This oxidative glutamate toxicity has a mechanistic association with AD as GSH reduction is accelerated in AD [42]. Next, the protective effect of OABL on glutamate-induced cytotoxicity in PC12 cells was detected. As observed in Fig. 2F, the cell viability treated with glutamate only was 67.1%, and treatment with OABL at a concentration of 10 μM rescued 75.9% of the cells, implying that the protective effect of OABL at least partly relates to oxytosis.

Ferroptosis is another cell death pathway closely related but not identical to oxytosis. The two forms of cell death due to oxidative stress are consequences of GSH depletion, ROS accumulation, including lipid peroxides, mitochondrial dysfunction, and the extracellular influx of Ca^{2+}. Distinct from oxytosis, oxidative stress in the ferroptosis can be induced downstream in the cascade by inhibition of glutathione peroxidase 4 (GPx4), a GSH-dependent antioxidant enzyme that loses activity under GSH depletion. However, the activity of GPx4 can be directly inhibited by the covalent interaction between a compound RSL3 with the active site selenocysteine of GPx4 [43]. As shown in Fig. 2G, OABL was neuroprotective against ferroptosis, and different concentrations of OABL (1, 5, 10 μM) significantly rescued 28.0%, 65.3%, and 70.8% of the cells, respectively, compared to the cell viability of 17.1% treated with RSL3 only. It revealed that OABL with the pronounced effects in neuroprotection at effective concentrations of < 20 μM could not

influence the GSH level in live cells.

Acetylcholinesterase (AChE) modulates cholinergic signal transmission through hydrolysis of acetylcholine (ACh), and AChE inhibitors are potential candidates for the development of drugs for the treatment of some neurodegenerative diseases, such as AD [44]. To assess the potential as AChE inhibitors, OABL and ABL were *in vitro* performed to assay the activity of inhibiting AChE based on Ellman's method. As shown in Fig. S3, the inhibition rate of the AChE positive inhibitor galantamine was 82.4%. However, neither OABL nor ABL has an observed anti-AChE effect, and the inhibition rates of OABL and ABL were 5.9% and 3.5%, respectively.

3.3. OABL attenuated the cognitive impairments in 6-month-old 5xFAD mice

To extend the *in vitro* studies, OABL was further evaluated regarding its protective effects against cognitive impairment in an AD mouse model, which are transgenic mice expressing 5 familial AD (FAD) mutation (5xFAD mice) [45]. A vehicle solution and OABL (20 mg/kg/day) were administered by intraperitoneal injection (*i.p.*) to 6-month-old WT and 5xFAD mice for 3 weeks and followed by a behavioral test (Fig. 3A). The body weight was evaluated in the vehicle or OABL-administered WT and 5xFAD mice to examine whether OABL exerts toxic effects on the mice. No significant changes were detected in body weight before (vehicle, 28.79 ± 0.73 g, n = 12; OABL, 29.06 ± 0.54 g; n = 12) and after the administration of vehicle or OABL (vehicle, 29.82 ± 0.73 g, n = 12; OABL, 30.19 ± 0.61 g; n = 12, Fig. S4A). These results indicate that the administration of OABL does not show toxicity in mice. Furthermore, there was no significant toxicity in the heart, liver, spleen, lung, and kidney by H&E staining shown in Fig. S4B.

The protective effects of OABL on the cognitive function in the 5xFAD mice were investigated by the Morris water maze (MWM) test. The track of the mice was shown in Fig. 3B. It is not obvious differences on day 1 and day 3, but on day 5, the escape latency of 5xFAD+Vehicle mice is higher than WT+Vehicle mice in Fig. 3C. 5xFAD+Vehicle group (52.52 ± 4.06 s) had longer escape latency compared to WT+Vehicle group (29.21 ± 4.32 s), indicating that 5xFAD mice exhibited cognitive and spatial memory loss. OABL treatment reduced escape latency in 5xFAD mice (32.81 ± 4.49 s) but not in the WT mice (48.78 ± 4.40 s). On the 6th day, the platform was removed to carry out a probe trial. There were significant differences between 5xFAD+Vehicle and WT+Vehicle mice. The results display that 5xFAD+Vehicle mice (11.85 ± 1.70 s, n = 4) spent less time in the target quadrant than WT+Vehicle mice (22.18 ± 1.97 s, n = 4). Although the difference was not presented between 5xFAD+Vehicle and 5xFAD+OABL groups, OABL treatment mice increased the time spent in the target quadrant in 5xFAD mice

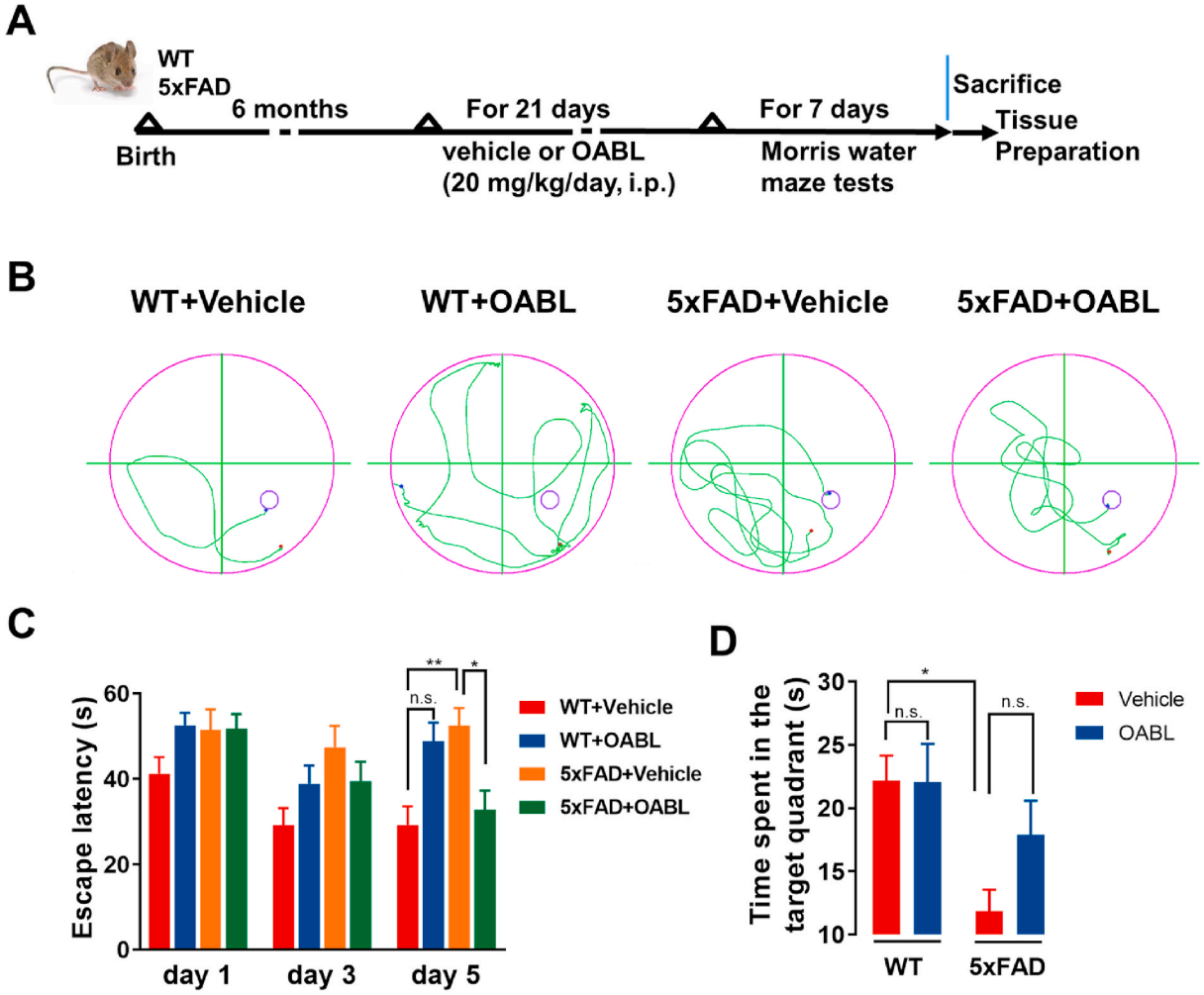

Fig. 3. OABL attenuated cognitive impairments in 5xFAD transgenic AD mice
(A) Experimental workflow of animal treatments (n = 8); **(B)** representative tracks of the test during the probe trial on day 5; **(C)** the escape latency of different groups on day 1, day 3, and day 5; **(D)** the time spent in target quadrant on day 6. The statistical analysis was performed via two-way ANOVA with Newman-Keuls multiple comparisons test, and the data are presented as the means ± SEM with significance different from each other (n = 6–8), (*) $p < 0.05$, (**) $p < 0.01$. n.s.: not significant.

(17.92 ± 2.68 s, Fig. 3D). Taken together, these results indicated that OABL rescued cognitive function impairments in 5xFAD mice.

3.4. Effects of OABL on preventing neuron damage and oxidative stress in 5xFAD mice

The accumulation of Aβ disrupts synaptic plasticity, further leading to neuron damage and memory loss in AD [46]. To investigate whether OABL could rescue the synapse and neuron impairment, the neuronal integrity and orderliness in the mice brain were performed by H&E staining to observe the histology of the cortex and hippocampal DG regions. Shrinkage of nuclei and shrinking neurons were found in 5xFAD mice shown in Fig. 4A, and administration of OABL could inhibit the mentioned above histopathological damages and recover the normal arrangement of neurons. The synapse structure and function were detected by transmission electron microscopy of ultra-structure of hippocampus synapse (Fig. 4B). OABL administration enhanced PSD length in 5xFAD mice hippocampus (OABL, 330.09 ± 15.27 nm; vs vehicle, 290.01 ± 5.43 nm; Fig. 4C). There was an increase in trends in 5xFAD+OABL mice hippocampus (59.16 ± 3.01 nm), compared to the 5xFAD+Vehicle mice (54.99 ± 3.61 nm) in Fig. 4D, although no significant differences of PSD width were observed among four groups. Besides, immunohistochemistry showed a similar result in the regions of hippocampal CA1, CA2, and CA3 in Fig. S5A. The results indicated that OABL treatment could rescue neuron damage and synapse dysfunction.

Oxidative stress is interrelated in the pathogenesis of AD. The decreased GSH level, the increased MDA content, and the fluctuant activity of SOD are associated with the aggregation of Aβ plaques and AD [47]. To explore whether OABL could have an impact on GSH, MDA and T-SOD, we quantified GSH, MDA levels and T-SOD activity in the cortex of 5xFAD mice brain. Lower GSH level indicated lower antioxidant level in 5xFAD mice brain than that in WT mice shown in Fig. 4E. OABL treatment increased the GSH level of 5xFAD mice. The MDA content was significantly higher in the cortex of 5xFAD+Vehicle mice (30.7 ± 1.6 nmol/mg prot) than that in WT+Vehicle mice (14.9 ± 0.8 nmol/mg prot) shown in Fig. 4F, illustrating that 5xFAD mice present with higher levels of free radicals and cellular damage. Interestingly, OABL treatment substantially reduced the MDA level of 5xFAD mice (20.3 ± 1.5 nmol/mg prot). Besides, in Fig. 4G, the T-SOD activity was also higher in the cortex of 5xFAD+Vehicle mice (153.92 ± 0.83 U/mg prot) than WT+Vehicle mice (130.55 ± 3.70 U/mg prot), and OABL treatment significantly reduced the T-SOD activity of 5xFAD mice (138.05 ± 1.40 U/mg prot). We also quantified MDA levels and T-SOD activity in the serum of 5xFAD mice. Similarly, the MDA and T-SOD contents significantly higher 5xFAD+Vehicle mice than that in WT+Vehicle mice shown in Figs. S5B and S5C. OABL treatment reduced the MDA and T-SOD levels of 5xFAD mice brain.

3.5. The benefit of OABL to decrease Aβ accumulation and p-Tau protein

5xFAD mice display an earlier onset and a more rapid rate of pathogenesis, which depends on Swedish mutation at the β-cleavage site and Florida and London mutations at the γ-cleavage site of APP, and two additional mutations of the PSEN1 gene [48]. The expression of β-secretase is associated with the production of Tau [49]. Hence, the level of BACE1 is important for further revealing the mechanism about effecting of OABL. Briefly, the expression of BACE1 protein in different groups was tested by Western blotting (Fig. 5A). The quantitative expression of BACE1 protein in 5xFAD+Vehicle group (0.64 ± 0.02) was obviously increased 2.7 times as much as in WT+Vehicle group (0.24 ± 0.04) in Fig. 5B. OABL-administration 5xFAD mice distinctly reduced the expression of BACE1 protein (0.34 ± 0.02). In the mRNA level of BACE1, 5xFAD+Vehicle mice showed 47% higher BACE1 level than WT+Vehicle mice in Fig. 5C. Likewise, OABL-administration 5xFAD mice displayed a decrease of BACE1 mRNA level in Fig. 5C.

The abnormal Aβ accumulation and hyperphosphorylated Tau (p-Tau) are the typical pathological characteristic of the AD brain. 5xFAD mice can exhibit higher Aβ and p-Tau concentrations than WT mice [50,51]. To assess the benefit of OABL in decreasing Aβ accumulation and p-Tau protein, the expression of $A\beta_{1\text{-}42}$ in the hippocampus and the level of p-Tau in the cortex of mice brain was determined respectively by ELISA kits. As shown in Fig. 5D and E, the levels of $A\beta_{1\text{-}42}$ were significantly higher in the 5xFAD+Vehicle group (930.93 ± 136.02 pg/mL), compared with WT+Vehicle group (169.87 ± 8.12 pg/mL). OABL amazingly decreased the abnormal accumulation of $A\beta_{1\text{-}42}$ in 5xFAD mice (472.93 ± 226.59 pg/mL) in Fig. 5D. For the protein level of p-Tau in the cortex of mice brain, 5xFAD+Vehicle group (67.36 ± 1.63 pg/mL) had higher concentration than WT+Vehicle group (47.89 ± 2.34 pg/mL). OABL-administration reduces the production of p-Tau in 5xFAD mice (56.96 ± 3.12 pg/mL, Fig. 5E). We also quantified the protein level of p-Tau in serum shown in Fig. S7B. 5xFAD+Vehicle group (13.11 ± 0.55 pg/mL) had higher concentration than WT+Vehicle group (10.78 ± 0.81 pg/mL). OABL-administration reduces the production of p-Tau in 5xFAD mice (9.17 ± 0.73 pg/mL). Furthermore, the amyloidogenesis in wildtype and 5xFAD mice brain was detected by thioflavin-S staining, which can dye Aβ by interacting with β sheet-rich structures of Aβ. As shown in Fig. 5F and Fig. S6A, the higher accumulation of amyloid plaques was detected in brain of 5xFAD+Vehicle mice, while only lower accumulation of Aβ was observed in OABL treatment 5xFAD mice. Immunofluorescence assay also uncovered that supplement with OABL could decrease Aβ aggregation in the hippocampus and cortex of the 5xFAD mice. As shown in Fig. 5G and Figs. S6B and S6C, the fluorescent signal of $A\beta_{1\text{-}42}$ in the 5xFAD+Vehicle group was significantly higher than the control group, and administration of OABL weakens the fluorescent strength of $A\beta_{1\text{-}42}$ in the 5xFAD+OABL group. Among them, CA1, CA2, and cortex regions had more obvious change between the 5xFAD+OABL group and the 5xFAD+Vehicle group. Similarly, the results of immunohistochemistry staining in the hippocampus and cortex showed that the inhibition of Aβ aggregation after OABL administration in 5xFAD mice Fig. S7. The results indicated OABL not only inhibited the expressions of $A\beta_{1\text{-}42}$ and p-Tau but also suppressed the expression of Aβ-related enzyme BACE1.

3.6. OABL attenuated the glial reactivation in 5xFAD mice

Gliosis is a characteristic of AD brains, and reactive astrocytes and microglia have been observed close to amyloid plaques [52]. We determined whether OABL had effects on GFAP and Iba-1, which are well-known gliosis markers. As shown in Fig. 6A and B, the fluorescent signal of GFAP was notably appeared in the 5xFAD+Vehicle group, and OABL treatment weakened the fluorescent strength of GFAP in the cortex and hippocampus regions of the 5xFAD+OABL group. However, this alteration is different in different regions of the hippocampus (Fig. 6A), such as CA1, CA2, CA3, and DG. The increase in GFAP protein expression was found to be attenuated in the CA1 and CA2 regions of the hippocampus but not in CA3 and DG after OABL administration in Fig. 6B. Besides, immunohistochemistry staining showed a similar result in the region of histology of the cortex and hippocampus CA1 in Fig. S8. In addition, western blotting indicated that the protein level of GFAP was increased in 5xFAD+vehicle mice (1.09 ± 0.23), compared with the level in WT+Vehicle mice (0.5 ± 0.05). OABL administration 5xFAD mice showed a reduced protein level of GFAP (0.25 ± 0.10) in the cortex of mice brain shown in Fig. 6C and D.

Furthermore, another marker for reactive microglia, Iba-1 protein was measured by immunofluorescence, immunohistochemistry, and western blotting in Fig. 7. OABL treatment weakened the fluorescent strength of Iba-1 in the cortex and the CA1, CA2, and CA3 regions of the hippocampus, but not in DG of 5xFAD mice in Fig. 7A and B. The similar result was showed in the cortex and hippocampus CA1 by immunohistochemistry staining (Fig. S9). Western blotting showed that the Iba-1 expression in 5xFAD+vehicle mice (0.88 ± 0.08) had a clear increase trend, compared with expression in WT+Vehicle mice (0.63 ± 0.04).

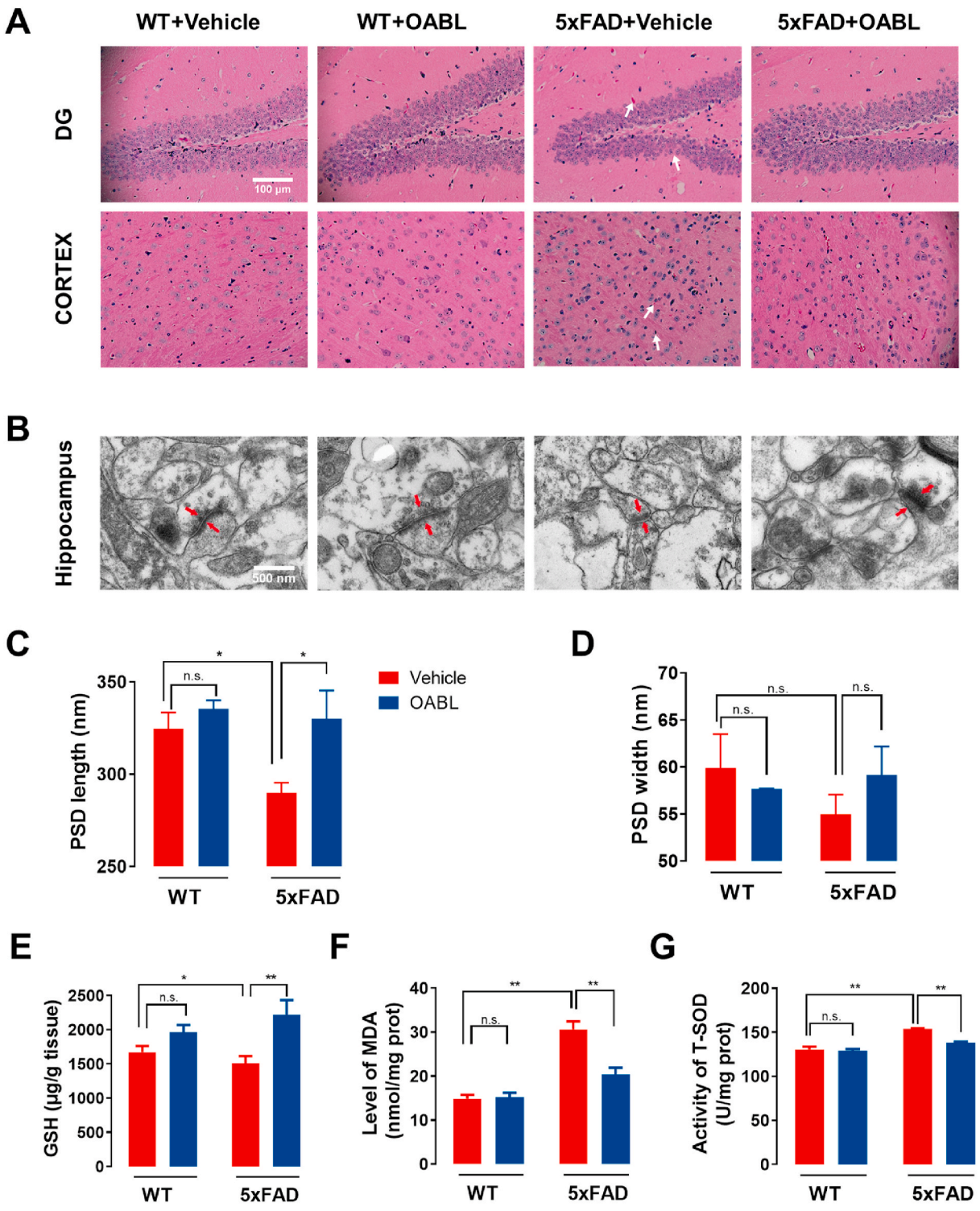

Fig. 4. OABL alleviated neuronal damage and oxidative stress in 5xFAD mice brain

(A) Representative images of H&E staining in DG region of hippocampus and cortex among experimental groups. The clear features of shrinkage of nuclei and shrinking neurons (white arrows) were improved in the 5xFAD+OABL group, compared with the 5xFAD+Vehicle group; **(B)** typical electron micrograph of synaptosomal sections from the hippocampus. The PSD is displayed with red arrows. Electron micrograph analyses were performed on 12 slices from 3 animals per group; **(C, D)** quantification of width and length of PSD based on electron micrography analyses by ImageJ software; **(E–G)** the levels of GSH, MDA and T-SOD in cortex (n = 7). GSH was determined by DTNB assay, MDA was determined by homogenizing the cortex in PBS with EDTA and then TBA test, and T-SOD was measured by hydroxylamine method. The statistical analysis was performed via two-way ANOVA with Newman-Keuls multiple comparisons test, and the data are presented as the means ± SEM with significance different from each other, (*) $p < 0.05$, (**) $p < 0.01$. n.s.: not significant. (For interpretation of the references to color in this figure legend, the reader is referred to the Web version of this article.)

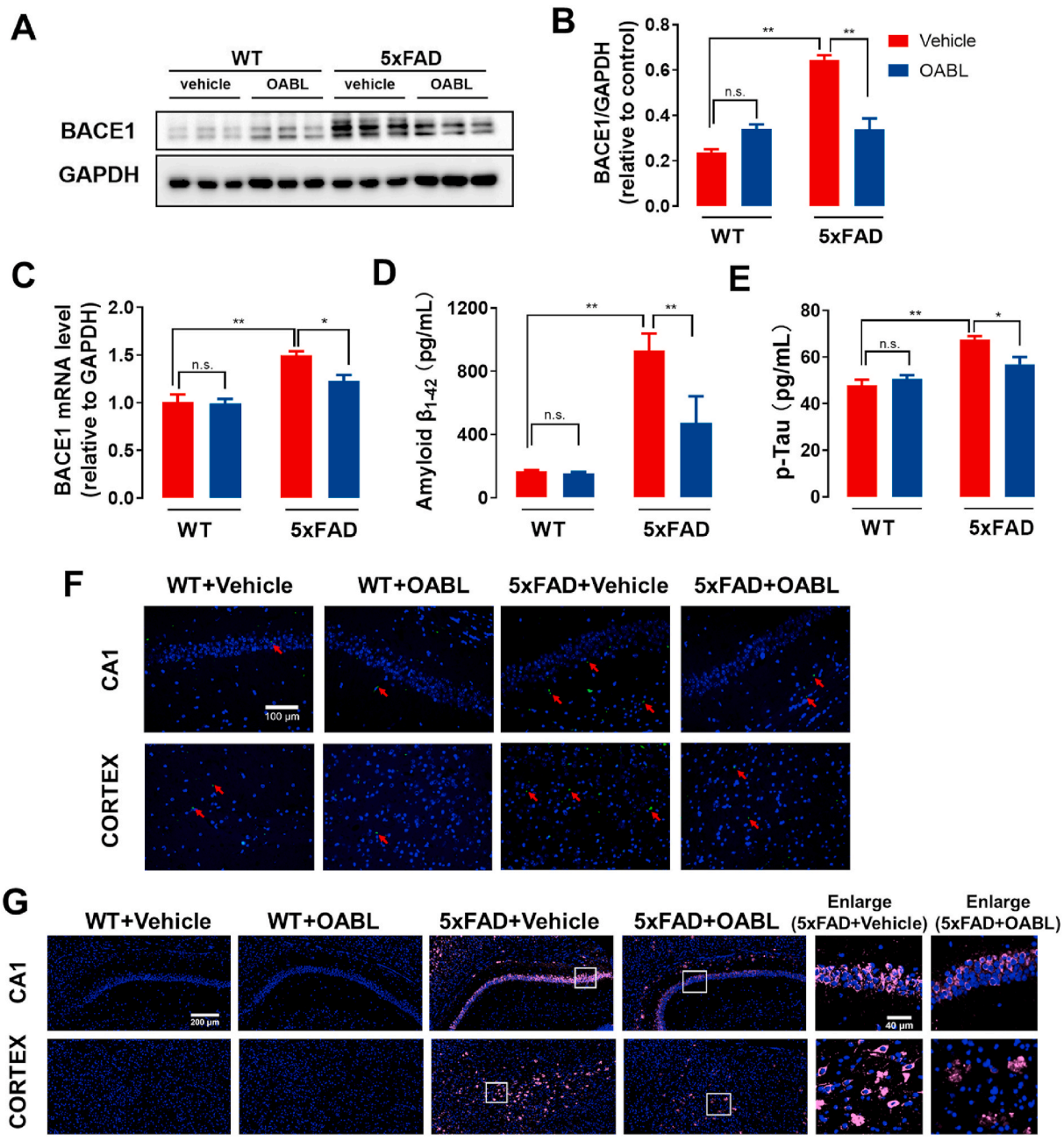

Fig. 5. OABL reduced the Aβ accumulation and the expression of p-Tau protein in 5xFAD mice brain
(A) Representative Western blots of BACE1 protein in the cortex of mice brain in different groups; **(B)** relative optical density (O.D.) of the BACE1 protein (n = 6); **(C)** the mRNA level of BACE1 in the cortex of mice brain by qRT-PCR (n = 6); **(D)** the level of $A\beta_{1\text{-}42}$ in the hippocampus of different groups (n = 8–10) measured by ELISA kit (R&D); **(E)** the level of p-Tau protein in the cortex of mice brain (n = 5–7) measured by ELISA kit (MLBio); **(F)** representative thioflavin S staining images for detection of Aβ accumulation and immunostaining of $A\beta_{1-42}$ in the hippocampus and cortex. Red arrows represent $A\beta_{1\text{-}42}$-positive amyloid plaques; **(G)** representative immunofluorescence images for detection of $A\beta_{1\text{-}42}$ (pink, Alexa Fluor® Plus 647) in the hippocampus and cortex. Nuclei was stained in blue (DAPI), and fluorescence intensity of $A\beta_{1\text{-}42}$ was analyzed in Supplementary data (Fig. S6C). The statistical analysis was performed via two-way ANOVA with Newman-Keuls multiple comparisons test, and the data are presented as the means ± SEM with significance different from each other, (*) $p < 0.05$, (**) $p < 0.01$. n.s.: not significant. (For interpretation of the references to color in this figure legend, the reader is referred to the Web version of this article.)

Moreover, OABL treatment distinctly decreased the expression in the cortex of 5xFAD mice brain (0.57 ± 0.07) in Fig. 7C and D.

3.7. Effects of OABL treatment on inflammatory responses in 5xFAD mice

Inflammation responses are increased in AD brains, and neuroinflammation can be induced by NF-κB activation. As an implication for amyloidogenesis, the activation of NF-κB in the brain can affect the development of AD [53]. Meanwhile, the activation of glial cells contributes to the release the proinflammatory factors. To verify the anti-inflammation effect of OABL in AD mice, the phosphorylation of NF-κB p65 in the hippocampus and cortex was detected. Immunofluorescence assay in Fig. 8A and B showed that OABL weakened the fluorescent signal of NF-κB p-p65 (green, FITC) in the cortex and four regions of the hippocampus of 5xFAD mice, compared with the 5xFAD+Vehicle mice. In addition, the levels of inflammatory mediators IL-1β and TNF-α in the serum of 5xFAD mice were assessed by RT-PCR. As shown in Fig. 8C and D, OABL treatment markedly decreased the

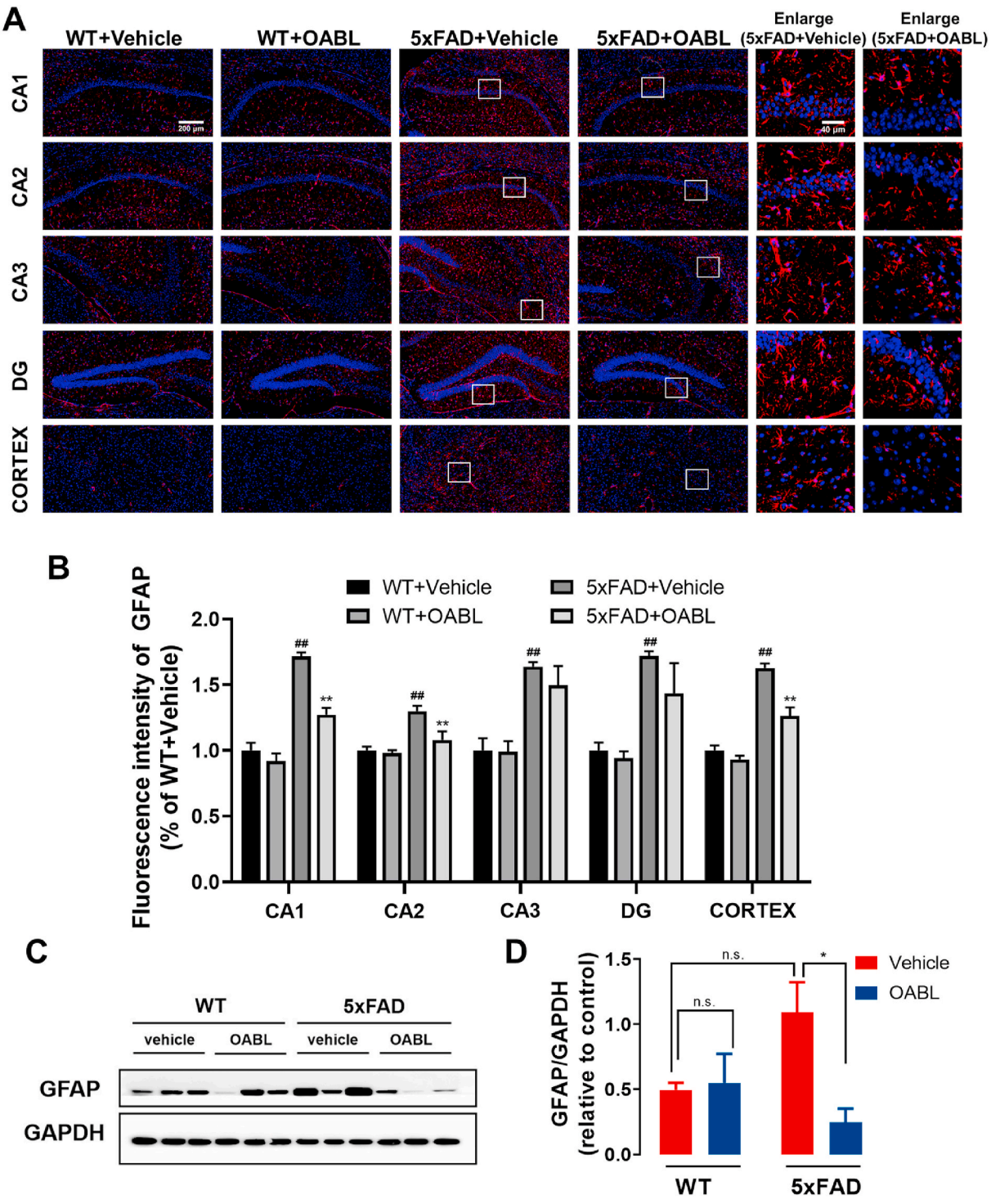

Fig. 6. OABL suppressed the astrogliosis in 5xFAD mice brain
(A) Representative immunofluorescence images for detection of GFAP (red, CY3) in the hippocampus and cortex of different groups. Nuclei were stained in blue (DAPI); **(B)** quantification of positive area based on immunofluorescence staining sections by ImageJ software. Sections statistical analysis of fluorescence intensity of GFAP protein was conducted on 12 slices from 3 animals per group, (##) $p < 0.01$; **(C)** representative Western blots of GFAP protein in the cortex of mice brain; **(D)** relative optical density of GFAP protein (n = 6). The statistical analysis was performed via two-way ANOVA with Newman-Keuls multiple comparisons test, and the data are presented as the means ± SEM with significance different from each other, (*) $p < 0.05$, (**) $p < 0.01$. n.s.: not significant. (For interpretation of the references to color in this figure legend, the reader is referred to the Web version of this article.)

mRNA levels of TNF-α and IL-1β in 5xFAD mice brain. The results indicated that OABL treatment effectively alleviated neuro-inflammation, perhaps by suppressing NF-κB activation in the brain of AD mice.

4. Discussion

As the single-target approach has not proven to be successful in the development of effective drugs against AD up to now, the development of multi-target treatments is highly necessary [54–57]. The

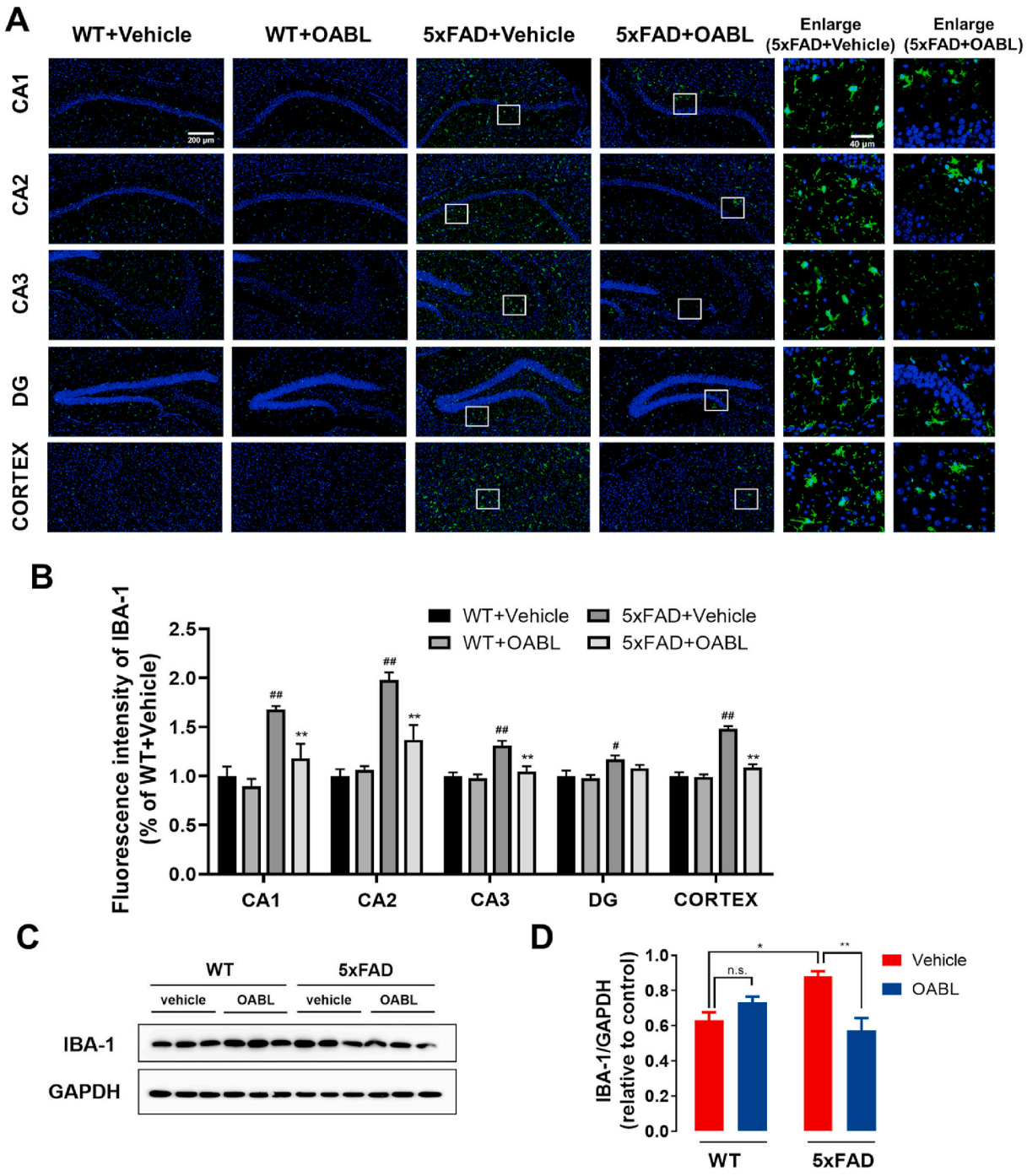

Fig. 7. OABL suppressed the over-activation of microglia in 5xFAD mice brain
(A) Representative immunofluorescence images for detection of Iba-1 (green, FITC) in the hippocampus and cortex of different groups. Nuclei was stained in blue (DAPI); **(B)** quantification of positive area based on immunofluorescence staining sections by ImageJ software. Sections statistical analysis of fluorescence intensity of Iba-1 protein was conducted on 12 slices from 3 animals per group, (##) $p < 0.01$; **(C)** representative Western blots of Iba-1 protein in the cortex of mice brain; **(D)** relative optical density of Iba-1 protein (n = 6). The statistical analysis was performed via two-way ANOVA with Newman-Keuls multiple comparisons test, and the data are presented as the means ± SEM with significance different from each other, (*) $p < 0.05$, (**) $p < 0.01$. n.s.: not significant. (For interpretation of the references to color in this figure legend, the reader is referred to the Web version of this article.)

microenvironment of early AD is characterized by inflammatory responses and oxidative stress, which precede the appearance of the amyloid cascade [7]. Inflammation is often accompanied by the activation of the immune system, which is ultimately mediated primarily by glial cells, such as microglia and astrocytes [58,59]. Among all non-neuronal CNS cells, microglia are thought to control the metabolic balance in the brain, including the secretion of pro-inflammatory or anti-inflammatory cytokines and phagocytosis of abnormal proteins [60]. Two major types of macrophages exist as the classical M1 phenotype, which can be activated by LPS or interferon-γ to trigger pro-inflammatory responses, and the alternate M2 phenotype, which is activated by increased IL-10, Arg-1 or IL-13 to execute anti-inflammatory effects [61–63]. NF-κB, a key transcription factor, promotes the proinflammatory M1 activation of microglia [64]. Recent studies have shown that targeting microglia may produce more beneficial therapeutic outcomes [13,65,66]. In this work, based on the phenotypic screening assay against microglia

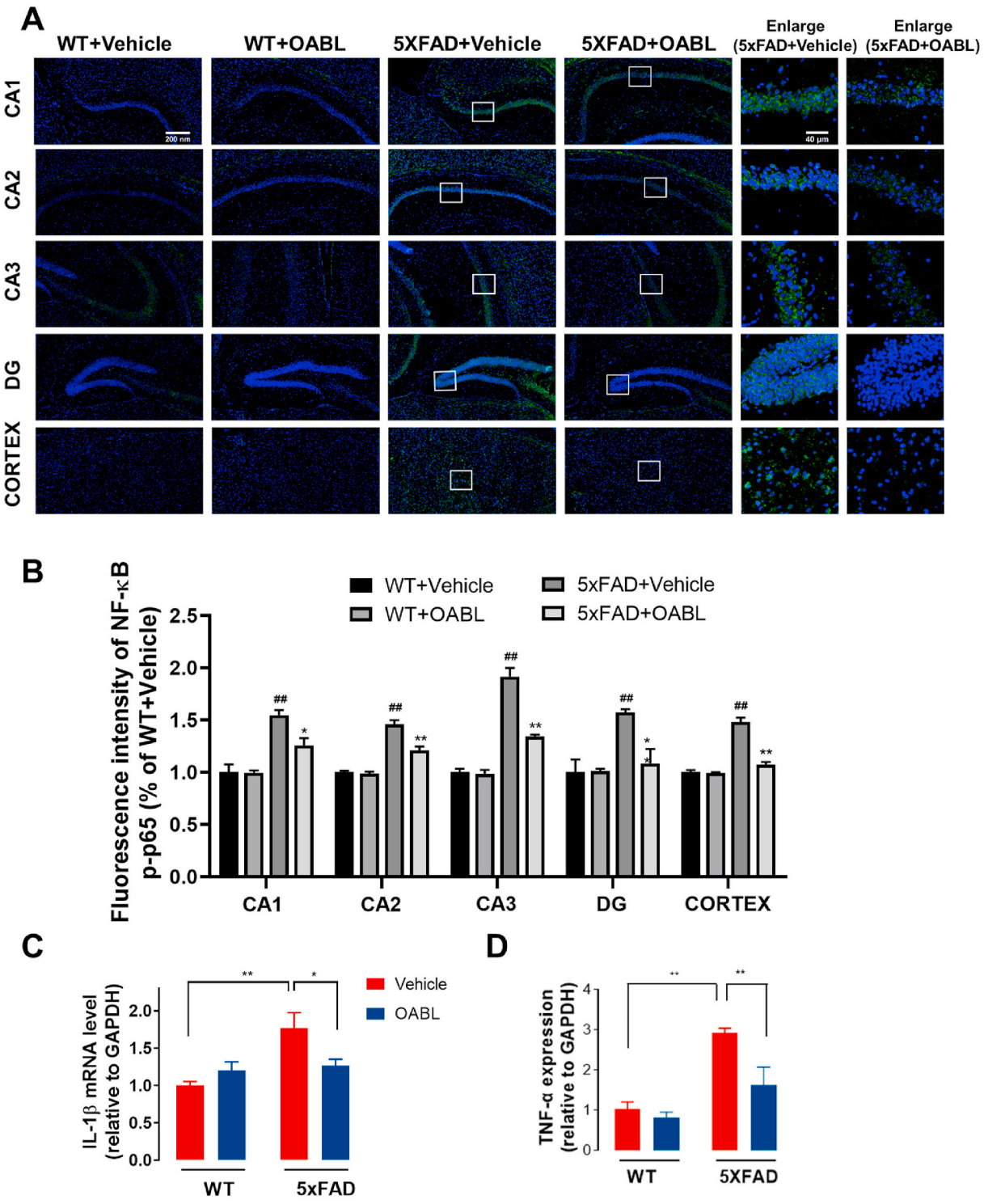

Fig. 8. OABL reduced the activation of the NF-κB transcriptional pathway in 5xFAD mice brain
(A) Representative immunofluorescence images for detection of NF-κB p-p65 (green, FITC) in the hippocampus and cortex. Nuclei were stained in blue (DAPI); **(B)** quantification of positive area based on immunofluorescence staining sections by ImageJ software. Sections statistical analysis of fluorescence intensity of NF-κB p-p65 was conducted on 12 slices from 3 animals per group, (##) $p < 0.01$; **(C, D)** the mRNA levels of IL-1β and TNF-α in the cortex of mice brain of different groups measured by qRT-PCR (n = 4). The statistical analysis was performed via two-way ANOVA with Newman-Keuls multiple comparisons test, and the data are presented as the means ± SEM with significance different from each other, (*) $p < 0.05$, (**) $p < 0.01$. (For interpretation of the references to color in this figure legend, the reader is referred to the Web version of this article.)

neuroinflammation, we firstly screened out a hit OABL with strong anti-neuroinflammatory effect, low cytotoxicity, good BBB penetration and ADMET properties from 4207 small compounds (Fig. 1 and Fig. S1). Furthermore, in the BV-2 cells model, we observed that LPS stimulation increased microglial M1-type inflammatory factors (including TNF-α, PGE_2, iNOS, COX-2, and NF-κB translocation), which could be reduced by OABL (Fig. 1). We also observed that OABL partly increased the expression of microglial M2-type factor IL-10 in BV-2 cells (Fig. 1). The

results indicated OABL possessed beneficial anti-inflammatory effects by targeting microglia.

Oxidative stress also contributes significantly to the pathogenesis and progression of AD in the early stage [14,67]. Prolonged or excessive microglial cell activation may produce cytokines, chemokines, and ROS, which sustain the oxidative microenvironment. ROS is a typical characteristic of oxidative stress and an essential initiator of neuronal damage. Brain tissue has an active metabolism rate, and thus, there are high amounts of ROS in the brain compared with the amounts in other organs [68]. Thus, eliminating the oxidative stress cascade reaction has been proven as a new perspective with significant great potential for early AD treatment. OABL was further measured by H_2O_2 and 6-OHDA-induced neuronal damage, oxytosis, and ferroptosis in the PC12 cell model. The results showed OABL possessed strong and pronounced neuroprotection effects (Fig. 2). The structure of OABL should lose the antioxidant effect due to the lack of hydroxyl groups. However, OABL exhibited cellular antioxidant capacity against H_2O_2 and 6-OHDA-induced neuronal damage, glutamate-induced oxytosis, and RSL3-induced ferroptosis (Fig. 2), implying that OABL might activate the antioxidant response element (ARE) of redox signaling. The existence of the characteristic α-methylene-γ-lactone motif is believed to be an essential pharmacophore, which could increase the Nrf2 levels because of molecules bearing a Michael system [69,70]. Our previous study showed that OABL and its derivatives could induce the antioxidant enzyme HO-1 [35]. Thus, OABL protects from oxidative stress-induced death via an indirect anti-oxidant mechanism. However, the exact pathways and target proteins mediating the neuroprotection effects of OABL remain unclear, and in future investigations, proteins of the Nrf2 pathway could be considered.

Reduced GSH can react with Michael acceptors such as the α,β-unsaturated carbonyl moiety, in which GSH is developing into a therapeutic objective for the treatment of oxidative stress-related disease [71]. The α-methylene-γ-lactone motif of OABL is a typical Michael acceptor, which can react rapidly with biomolecules containing the naked –SH group [72]. In our study, OABL can react with GSH in PBS and largely form an OABL-GSH adduct within 2 h at 37 °C, but not influence the cellular GSH level and cell proliferation within 2 h and 24 h treatment of OABL at < 20 μM (Fig. 2). It indicated that the pronounced effects of anti-inflammatory and neuroprotection of OABL at effective concentrations of < 20 μM were irrelevant to GSH level in live cells. This OABL-GSH adduct did not show any protective effect on the oxidative damage in PC12 cells at the 20 μM. Besides, acetylcholinesterase (AChE) inhibitors are very successful drugs for the treatment of AD. Four FDA-approved inhibitors (tacrine, donepezil, rivastigmine, and galantamine) can delay AD symptoms but are not fundamental AD treatments [73]. Our *in vitro* experiments showed that neither OABL nor ABL had a potential anti-AChE effect.

During AD development, pathological Aβ and Tau accumulate and mislocalize to synapses, leading to synaptic dysfunction and neuronal damage [74–76]. In addition, increased microglial engulfment of synapses was found in AD patients and transgenic mice, which is related to the decrease in synapse density [77]. Our results revealed that OABL significantly prevented neuron impairment and restored the levels of PSD95, thus rescuing neuron loss in 5xFAD mice brain (Fig. 4). Oxidative stress is a potential factor in the development of AD, which is considered to be an imbalance between the level of antioxidant defense and the production of free radicals that can cause potential brain damage. The GSH redox cycle is extremely important in the detoxification of free radical in the brain tissue, and GSH showed a decreased level in AD brain. OABL demonstrated antioxidant activity by significantly increasing GSH level in 5xFAD mice brain. An increase in SOD activity usually indicates enhanced protection against oxidative stress and injury [78]. However, during the early stages of the inflammatory response (compensatory phase), SOD activity is known to increase owing to the excessive production of free radicals [47]. As a final metabolite of lipid peroxidation, MDA reflects the levels of free radicals and cellular damage (higher lipid peroxidation correlates to higher levels of MDA) [79]. As anticipated, increased MDA level and SOD activity were found in the cortex and serum of 5xFAD mice, suggesting that although these animals may suffer from oxidative stress-induced damage, they are likely to stay in the compensatory phase. Interestingly, OABL attenuated both MDA level and SOD activity, indicating a beneficial effect on oxidative stress.

Aβ accumulation and hyperphosphorylated Tau (p-tau) are two major pathological indicators of AD. Numerous studies imply the presence of crosstalk between Aβ or p-tau and various molecular signaling pathways, but the exact mechanism of how Aβ enhances the pathogenesis of AD has not been fully elucidated [80,81]. Oxidative stress and neuroinflammation were demonstrated to be associated with neuronal loss and cognitive deficits. Meanwhile, the excessive Aβ and p-tau accumulation can lead to much more oxidative stress and inflammation, which can produce a vicious cycle to aggravate the neural damage. To identify the therapeutic potential of OABL in AD, 6-months 5xFAD mice model with obvious cognitive impairments were *i.p.* administrated by OABL (20 mg/kg/day). The administration of OABL for 21 days exerted attenuating effects on the cognitive impairments in 5xFAD mice by the Morris water maze test (Fig. 3). OABL treatment did not have adverse effects at the effective dose. Then, we examined the effects of OABL on neuropathological changes in AD. The protein levels of Aβ and p-tau were evaluated in the brain tissue of mice in the 5xFAD group (Fig. 5). The administration of OABL reduced the protein levels of Aβ and p-tau, as well as the number of amyloid plaques. OABL may delay the formation of amyloid plaques more effectively by inhibiting the accumulation of ROS. There is a possibility that OABL may affect APP processing, Aβ, and p-Tau production by alleviating oxidative stress in the brain. Oxidative stress has been shown in a wide range of studies to up-regulates BACE-1 expression or increases γ-secretase activity, both of which are major APP-cleaving enzymes of Aβ production [82,83]. To verify this hypothesis, the protein level of BACE1 in the cortex was examined to determine whether OABL affects the Aβ production. The administration of OABL downregulated the protein and mRNA level of BACE1 in 5xFAD mice.

Activated astrocytes and microglia are found around dense amyloid plaques in the brains of AD patients [84,85]. GFAP and Iba-1 are markers of reactive astrocytes and microglia [86,87], respectively, which were downregulated in the hippocampus and cortex of 5xFAD+OABL mice compared with 5xFAD+vehicle mice, as shown by immunofluorescence and western blotting and (Figs. 6 and 7). The immunoreactivity of GFAP and Iba-1 were decreased in the CA1, CA2, and cortex of 5xFAD+OABL mice compared with 5xFAD+vehicle mice. However, the immunoreactivity of GFAP was not decreased in the CA3 and DG regions, while that of Iba-1 was decreased in the CA3 but not in the DG region of the hippocampus in 5xFAD+OABL mice. The number of both astrocytes and microglia are reported to be differential in the different brain regions. For example, the density of astrocytes is higher in CA3 than in CA1, but on the contrary, the density of microglia is higher in the CA1 than in the CA3 region [88]. It is possible that the differential attenuating effects of OABL on the reactive astrocytes and microglia in the different regions is due to the differential population of astrocytes and microglia.

As an implicator for amyloid production, the activation of NF-κB in the brain can affect the development of AD. Many NF-κB inhibitors ameliorate the development of AD by reducing amyloid [53]. We found that the immunoreactivity of NF-κB p-p65 was markedly decreased in the hippocampus and cortex of 5xFAD+OABL mice compared with 5xFAD+vehicle mice (Fig. 8), which is consistent with the suppression of NF-κB p65. In addition, reactive astrocytes and microglia from 5xFAD mouse model [89] are known to release pro-inflammatory cytokines, such as IL-1β and TNF-α [90]. IL-1β was previously shown to induce reactive astrogliosis, contributing to astrocyte-mediated neuronal death; moreover, its levels are increased in AD brains. To investigate the effects of OABL on cytokines, the mRNA levels of IL-1β and TNF-α were

investigated in the brain of the 4 groups. The mRNA levels of IL-1β and TNF-α were increased in 5xFAD+vehicle mice compared with WT-vehicle mice, and these increases were significantly attenuated in the 5xFAD+OABL mice. The attenuation of the reactive astrocytes and microglia and the suppression of NF-κB activation are thought to cause the decrease in the mRNA levels of IL-1β and TNF-α in 5xFAD+OABL mice. Based on these results, it can be concluded that OABL reduced the neuroinflammation induced by amyloid plaques in 5xFAD mice.

α-Methylene-γ-lactone moiety of STLs is the most essential structural feature for the anti-inflammatory and cytotoxic activities but also for side effects, e.g., allergic effects [91]. The current study provides more options for pharmacologists to develop anti-AD agents. OABL may have perspectives for the future, but importantly, its advantages must be carefully considered for use as therapeutics. Especially, OABL distinctly decreased the expressions of BACE1 and Iba-1 proteins in brain from 5xFAD transgenic mice, but at the same time OABL tended to increase the BACE1 and Iba-1 proteins levels in wild type mice. Especially, OABL distinctly decreased the expressions of BACE1 and Iba-1 proteins in brain from 5xFAD transgenic mice, but at the same time OABL tended to increase the BACE1 and Iba-1 proteins levels in wild type mice. Therefore, the toxicity of OABL in healthy objects, as well as its absorption, distribution in different organs, including liver, gut, and brain, should be further determined in the future study.

5. Conclusion

Overall, in the present study, we phenotypically screened the anti-neuroinflammation effects from the compounds library and found that natural product OABL was able to suppress neuroinflammation and exhibit pronounced neuroprotection effects *in vitro*, as well as being capable of penetrating the blood-brain barrier. In *in vivo* study, the administration of OABL for 3 weeks attenuated the impairments in cognitive function observed in APP/PSEN1 transgenic (5xFAD) mice without apparent toxicity. The OABL-administration in 5xFAD mice caused a reduction in the number of amyloid plaques and in the protein levels of Aβ and p-tau as well as BACE1. OABL also restored the reduction in the number of mature spines and the PSD95 in the hippocampus and cortex of 5xFAD mice. In addition, OABL-administered 5xFAD mice displayed lower levels of GFAP and Iba-1, TNF-α and IL-1β, and SOD and MDA in the brains compared with vehicle-administered 5xFAD mice. The results shed light on the potential of the natural product OABL as a novel lead with potential use for AD drug discovery due to its multi-targets profile.

Author contributions

Jiang-Jiang Tang, Lan-Fang Huang, and Zhigang Liu conceived and designed the experiments. Jiang-Jiang Tang, Lan-Fang Huang, Yi-Meng Wang, Jia-Le Deng, and Xiao-Na Peng performed the experiments. Jiang-Jiang Tang and Lan-Fang Huang analyzed the data. Cong Guo, Zhigang Liu, and Jin-Ming Gao contributed reagents/materials/analysis tools. Lan-Fang Huang, Jiang-Jiang Tang, and Zhigang Liu wrote the draft and checked and revised it. All authors approved to submit this version to this publication.

Declaration of competing interest

The authors declare that they have no known competing financial interests or personal relationships that could have appeared to influence the work reported in this paper.

Acknowledgments

This work was supported by the National Natural Science Foundation of China (82073730 and 81871118) and the Science and Technology Department, Shaanxi Province (2020NY-153). The authors would like to thank Ms. Ping Xiang from NWAFU for HPLC-MS analysis and Ms. Fang-Ting Ma from TargetMol Co. for providing the natural products library. Dr. Zhigang Liu is also funded by the Alexander von Humboldt-Stiftung in Germany.

Appendix A. Supplementary data

Supplementary data to this article can be found online at https://doi.org/10.1016/j.redox.2022.102229.

References

[1] S.F.K. Lubeek, E.R. van der Geer, M.M.H.J. van Gelder, P.C.M. van de Kerkhof, M.J. P. Gerritsen, Improving dermatological Care for elderly people living in permanent healthcare institutions: suggestions from Dutch dermatologists, Acta Derm. Venereol. 96 (2016) 253–254.
[2] D.R. Elmaleh, M.R. Farlow, P.S. Conti, R.G. Tompkins, L. Kundakovic, R.E. Tanzi, Developing effective Alzheimer's disease therapies: clinical experience and future directions, J. Alzheimers Dis. 71 (2019) 715–732.
[3] R. van der Kant, L.S.B. Goldstein, R. Ossenkoppele, Amyloid-beta-independent regulators of tau pathology in Alzheimer disease, Nat. Rev. Neurosci. 21 (2020) 21–35.
[4] M. Tolar, S. Abushakra, J.A. Hey, A. Porsteinsson, M. Sabbagh, Aducanumab, gantenerumab, BAN2401, and ALZ-801-the first wave of amyloid-targeting drugs for Alzheimer's disease with potential for near term approval, Alzheimer's Res. Ther. 12 (2020) 95.
[5] S.Y. Hung, W.M. Fu, Drug candidates in clinical trials for Alzheimer's disease, J. Biomed. Sci. 24 (2017) 47.
[6] M.T. Heneka, M.J. Carson, J. El Khoury, G.E. Landreth, F. Brosseron, D.L. Feinstein, A.H. Jacobs, T. Wyss-Coray, J. Vitorica, R.M. Ransohoff, K. Herrup, S.A. Frautschy, B. Finsen, G.C. Brown, A. Verkhratsky, K. Yamanaka, J. Koistinaho, E. Latz, A. Halle, G.C. Petzold, T. Town, D. Morgan, M.L. Shinohara, V.H. Perry, C. Holmes, N.G. Bazan, D.J. Brooks, S. Hunot, B. Joseph, N. Deigendesch, O. Garaschuk, E. Boddeke, C.A. Dinarello, J.C. Breitner, G.M. Cole, D.T. Golenbock, M. P. Kummer, Neuroinflammation in Alzheimer's disease, Lancet Neurol. 14 (2015) 388–405.
[7] D.A. Butterfield, B. Halliwell, Oxidative stress, dysfunctional glucose metabolism and Alzheimer disease, Nat. Rev. Neurosci. 20 (2019) 148–160.
[8] S. Liao, J.N. Wu, R.M. Liu, S.X. Wang, J. Luo, Y. Yang, Y.N. Qin, T. Li, X.P. Zheng, J. Song, X.F. Zhao, C.N. Xiao, Y.J. Zhang, L.J. Bian, P. Jia, Y.J. Bai, X.H. Zheng, A novel compound DBZ ameliorates neuroinflammation in LPS-stimulated microglia and ischemic stroke rats: role of Akt(Ser473)/GSK3 beta (Ser9)-mediated Nrf2 activation, Redox Biol. 36 (2020) 101644.
[9] H. Sarlus, M.T. Heneka, Microglia in Alzheimer's disease, J. Clin. Invest. 127 (2017) 3240–3249.
[10] S.S. Jiao, X.Q. Yao, Y.H. Liu, Q.H. Wang, F. Zeng, J.J. Lu, J. Liu, C. Zhu, L.L. Shen, C.H. Liu, Y.R. Wang, G.H. Zeng, A. Parikh, J. Chen, C.R. Liang, Y. Xiang, X.L. Bu, J. Deng, J. Li, J. Xu, Y.Q. Zeng, X. Xu, H.W. Xu, J.H. Zhong, H.D. Zhou, X.F. Zhou, Y.J. Wang, Edaravone alleviates Alzheimer's disease-type pathologies and cognitive deficits, Proc. Natl. Acad. Sci. U. S. A. 112 (2015) 5225–5230.
[11] J.H. Wang, X. Lei, X.R. Cheng, X.R. Zhang, G. Liu, J.P. Cheng, Y.R. Xu, J. Zeng, W. X. Zhou, Y.X. Zhang, LW-AFC, a new formula derived from Liuwei Dihuang decoction, ameliorates behavioral and pathological deterioration via modulating the neuroendocrine-immune system in PrP-hA beta PPswe/PS1(Delta E9) transgenic mice, Alzheimer's Res. Ther. 8 (2016) 57.
[12] R.Y. Pan, J. Ma, X.X. Kong, X.F. Wang, S.S. Li, X.L. Qi, Y.H. Yan, J.B. Cheng, Q. S. Liu, W.Z. Jin, C.H. Tan, Z.Q. Yuan, Sodium rutin ameliorates Alzheimer's disease-like pathology by enhancing microglial amyloid-beta clearance, Sci. Adv. 5 (2019), eaau6328.
[13] S. Gunesch, M. Hoffmann, C. Kiermeier, W. Fischer, A.F.M. Pinto, T. Maurice, P. Maher, M. Decker, 7-O-Esters of taxifolin with pronounced and overadditive effects in neuroprotection, anti-neuroinflammation, and amelioration of short-term memory impairment in vivo, Redox Biol. 29 (2020).
[14] C. Cheignon, M. Tomas, D. Bonnefont-Rousselot, P. Faller, C. Hureau, F. Collin, Oxidative stress and the amyloid beta peptide in Alzheimer's disease, Redox Biol. 14 (2018) 450–464.
[15] T.F. Jiang, Q. Sun, S.D. Chen, Oxidative stress: a major pathogenesis and potential therapeutic target of antioxidative agents in Parkinson's disease and Alzheimer's disease, Prog. Neurobiol. 147 (2016) 1–19.
[16] Y.F. Lu, Z.Y. Guo, Y.J. Zhang, C. Li, Y. Zhang, Q. Guo, Q.J. Chen, X.L. Chen, X. He, L.S. Liu, C.H. Ruan, T. Sun, B. Ji, W.G. Lu, C. Jiang, Microenvironment remodeling micelles for Alzheimer's disease therapy by early modulation of activated microglia, Adv. Sci. 6 (2019) 1801586.
[17] J.R. Sundaram, C.P. Poore, N.H. Bin Sulaimee, T. Pareek, W.F. Cheong, M.R. Wenk, H.C. Pant, S.A. Frautschy, C.M. Low, S. Kesavapany, Curcumin ameliorates neuroinflammation, neurodegeneration, and memory deficits in p25 transgenic mouse model that bears hallmarks of Alzheimer's disease, J. Alzheimers Dis. 60 (2017) 1429–1442.
[18] M. Zabel, A. Nackenoff, W.M. Kirsch, F.E. Harrison, G. Perry, M. Schrag, Markers of oxidative damage to lipids, nucleic acids and proteins and antioxidant enzymes activities in Alzheimer's disease brain: a meta-analysis in human pathological specimens, Free Radical Biol. Med. 115 (2018) 351–360.

[19] Y. Dgachi, O. Sokolov, V. Luzet, J. Godyn, D. Panek, A. Bonet, H. Martin, I. Iriepa, I. Moraleda, C. Garcia-Iriepa, J. Janockova, L. Richert, O. Soukup, B. Malawska, F. Chabchoub, J. Marco-Contelles, L. Ismaili, Tetrahydropyranodiquinolin-8-amines as new, non hepatotoxic, antioxidant, and acetylcholinesterase inhibitors for Alzheimer's disease therapy, Eur. J. Med. Chem. 126 (2017) 576–589.

[20] C. Purslow, Mitochondria-targeted antioxidants: a potential new therapy for Alzheimer's disease? Expert Rev. Neurother. 12 (2012) 116. -116.

[21] Y. Feng, X.C. Wang, Antioxidant therapies for Alzheimer's disease, Oxid. Med. Cell Longev. 2012 (2012) 472932.

[22] J.M. Rubio-Perez, J.M. Morillas-Ruiz, A review: inflammatory process in Alzheimer's disease, role of cytokines, Sci. World J. 2012 (2012) 756357.

[23] D.C. Swinney, Phenotypic vs. Target-based drug discovery for first-in-class medicines, Clin. Pharmacol. Ther. 93 (2013) 299–301.

[24] W. Fischer, A. Currais, Z.B. Liang, A. Pinto, P. Maher, Old age-associated phenotypic screening for Alzheimer's disease drug candidates identifies sterubin as a potent neuroprotective compound from Yerba santa, Redox Biol. 21 (2019) 101089.

[25] A.J. Garcia-Pineres, M.T. Lindenmeyer, I. Merfort, Role of cysteine residues of p65/NF-kappa B on the inhibition by the sesquiterpene lactone parthenolide and-N-ethyl maleimide, and on its transactivating potential, Life Sci. 75 (2004) 841–856.

[26] S.B. Erel, S. Demir, A. Nalbantsoy, P. Ballar, S. Khan, N.U.K. Yavasoglu, C. Karaalp, Bioactivity screening of five Centaurea species and in vivo anti-inflammatory activity of C. athoa, Pharm. Biol. 52 (2014) 775–781.

[27] L.M. Bedoya, M.J. Abad, P. Bermejo, The role of parthenolide in intracellular signalling processes: review of current knowledge, Curr. Signal Transduct. Ther. 3 (2008) 82–87.

[28] Y.M. Zhao, M.L. Zhang, O.W. Shi, H. Kiyota, Chemical constituents of plants from the genus Inula, Chem. Biodivers. 3 (2006) 371–384.

[29] M. Han, J.-k. Wen, B. Zheng, D.-Q. Zhang, Acetylbritannilatone suppresses NO and PGE 2 synthesis in RAW 264.7 macrophages through the inhibition of iNOS and COX-2 gene expression, Life Sci. 75 (2004) 675–684.

[30] S. Dong, J.-J. Tang, C.-C. Zhang, J.-M. Tian, J.-T. Guo, Q. Zhang, H. Li, J.-M. Gao, Semisynthesis and in vitro cytotoxic evaluation of new analogues of 1-O-acetyl-britannilactone, a sesquiterpene from *Inula britannica*, Eur. J. Med. Chem. 80 (2014) 71–82.

[31] Y.J. Wang, X.Q. Chai, M. Han, J.K. Wen, Inhibition of l-*O*-acetylbritannilactone on expression of COX-2 and NF-κB in rats hippocampus with AD, Chin. Pharmacol. Bull. 24 (2008) 437–440.

[32] B.-N. Zhou, N.-S. Bai, L.-Z. Lin, G. Cordell, Sesquiterpene lactones from *Inula britannica*, Phytochemistry 34 (1993) 249–252.

[33] Q.-R. He, J.-J. Tang, Y. Liu, Z.-F. Chen, Y.-X. Liu, H. Chen, D. Li, Z.-F. Yi, J.-M. Gao, The natural product trienomycin A is a STAT3 pathway inhibitor that exhibits potent in vitro and in vivo efficacy against pancreatic cancer, Br. J. Pharmacol. 178 (2021) 2496–2515.

[34] A. Konczol, J. Muller, E. Foldes, Z. Beni, K. Vegh, A. Kery, G.T. Balogh, Applicability of a blood-brain barrier specific artificial membrane permeability assay at the early stage of natural product-based CNS drug discovery, J. Nat. Prod. 76 (2013) 655–663.

[35] J.-J. Tang, M.-R. Wang, S. Dong, L.-F. Huang, Q.-R. He, J.-M. Gao, 1,10-Seco-Eudesmane sesquiterpenoids as a new type of anti-neuroinflammatory agents by suppressing TLR4/NF-κB/MAPK pathways, Eur. J. Med. Chem. 224 (2021) 113713.

[36] N. Asiimwe, S.G. Yeo, M.S. Kim, J. Jung, N.Y. Jeong, Nitric oxide: exploring the contextual link with Alzheimer's disease, Oxid. Med. Cell Longev. 2016 (2016) 7205747.

[37] G.M. Barton, R. Medzhitov, Toll-like receptor signaling pathways, Science 300 (2003) 1524–1525.

[38] Y.P. Liu, J.K. Wen, Y.B. Wu, J. Zhang, B. Zheng, D.Q. Zhang, M. Han, 1,6-O, O-diacetylbritannilactones inhibits I kappa B kinase beta-dependent NF-kappa B activation, Phytomedicine 16 (2009) 156–160.

[39] J.J. Tang, S. Dong, Y.Y. Han, M. Lei, J.M. Gao, Synthesis of 1-O-acetylbritanni-lactone analogues from *Inula britannica* and in vitro evaluation of their anticancer potential, Med. Chem. Comm. 5 (2014) 1584–1589.

[40] P.C. Trippier, K.J. Labby, D.D. Hawker, J.J. Mataka, R.B. Silverman, Target- and mechanism-based therapeutics for neurodegenerative diseases: strength in numbers, J. Med. Chem. 56 (2013) 3121–3147.

[41] B. Wiatrak, A. Kubis-Kubiak, A. Piwowar, E. Barg, PC12 cell line: cell types, coating of culture vessels, differentiation and other culture conditions, Cells 9 (2020) 958.

[42] L. Huang, D.B. McClatchy, P. Maher, Z.B. Liang, J.K. Diedrich, D. Soriano-Castell, J. Goldberg, M. Shokhirev, J.R. Yates, D. Schubert, A. Currais, Intracellular amyloid toxicity induces oxytosis/ferroptosis regulated cell death, Cell Death Dis. 11 (2020) 828.

[43] W.S. Yang, K.J. Kim, M.M. Gaschler, M. Patel, M.S. Shchepinov, B.R. Stockwell, Peroxidation of polyunsaturated fatty acids by lipoxygenases drives ferroptosis, Proc. Natl. Acad. Sci. U. S. A. 113 (2016) E4966–E4975.

[44] J.P.S. Ferreira, H.M.T. Albuquerque, S.M. Cardoso, A.M.S. Silva, V.L.M. Silva, Dual-target compounds for Alzheimer's disease: natural and synthetic AChE and BACE-1 dual-inhibitors and their structure-activity relationship (SAR), Eur. J. Med. Chem. 221 (2021) 113492.

[45] Q. Liu, Y.J. Xi, Q.X. Wang, J.H. Liu, P.R. Li, X. Meng, K. Liu, W.X. Chen, X.B. Liu, Z. G. Liu, Mannan oligosaccharide attenuates cognitive and behavioral disorders in the 5xFAD Alzheimer's disease mouse model via regulating the gut microbiota-brain axis, Brain Behav. Immun. 95 (2021) 330–343.

[46] M.S. Parihar, G.J. Brewer, Amyloid-beta as a modulator of synaptic plasticity, J. Alzheimers Dis. 22 (2010) 741–763.

[47] W.W. Zhou, S. Lu, Y.J. Su, D. Xue, X.L. Yu, S.W. Wang, H. Zhang, P.X. Xu, X.X. Xie, R.T. Liu, Decreasing oxidative stress and neuroinflammation with a multifunctional peptide rescues memory deficits in mice with Alzheimer disease, Free Radical Biol. Med. 74 (2014) 50–63.

[48] G. Esquerda-Canals, L. Montoliu-Gaya, J. Güell-Bosch, S. Villegas, Mouse models of Alzheimer's disease, J. Alzheimers Dis. 57 (2017) 1171–1183.

[49] D. Sepulveda-Falla, L. Chavez-Gutierrez, E. Portelius, J.I. Velez, S. Dujardin, A. Barrera-Ocampo, F. Dinkel, C. Hagel, B. Puig, C. Mastronardi, F. Lopera, B. T. Hyman, K. Blennow, M. Arcos-Burgos, B. de Strooper, M. Glatzel, A multifactorial model of pathology for age of onset heterogeneity in familial Alzheimer's disease, Acta Neuropathol. 141 (2021) 217–233.

[50] T. Kanno, A. Tsuchiya, T. Nishizaki, Hyperphosphorylation of Tau at Ser396 occurs in the much earlier stage than appearance of learning and memory disorders in 5XFAD mice, Behav. Brain Res. 274 (2014) 302–306.

[51] W.A. Eimer, R. Vassar, Neuron loss in the 5XFAD mouse model of Alzheimer's disease correlates with intraneuronal A beta(42) accumulation and Caspase-3 activation, Mol. Neurodegener. 8 (2013) 2.

[52] A. Serrano-Pozo, A. Muzikansky, T. Gomez-Isla, J.H. Growdon, R.A. Betensky, M. P. Frosch, B.T. Hyman, Differential relationships of reactive astrocytes and microglia to fibrillar amyloid deposits in Alzheimer disease, J. Neuropathol. Exp. Neurol. 72 (2013) 462–471.

[53] C. Ju Hwang, D.Y. Choi, M.H. Park, J.T. Hong, NF-kappaB as a key mediator of brain inflammation in Alzheimer's disease, CNS Neurol. Disord. Drug Targets 18 (2019) 3–10.

[54] K.R. Wang, J. Shi, Y. Zhou, Y. He, J. Mi, J. Yang, S. Liu, X.C. Tang, W.M. Liu, Z. H. Tan, Z.P. Sang, Design, synthesis and evaluation of cinnamic acid hybrids as multi-target-directed agents for the treatment of Alzheimer's disease, Bioorg. Chem. 112 (2021) 104879.

[55] Y.X. Zhang, Y.L. Liu, Y.J. Tang, D. Zhang, H.C. He, J. Wu, J. Zheng, Antimicrobial alpha-defensins as multi-target inhibitors against amyloid formation and microbial infection, Chem. Sci. 12 (2021) 9124–9139.

[56] P.X. Liu, T.Y. Zhang, Q.J. Chen, C. Li, Y.C. Chu, Q. Guo, Y.W. Zhang, W.X. Zhou, H. Y. Chen, Z. Zhou, Y. Wang, Z.H. Zhao, Y.F. Luo, X.W. Li, H.L. Song, B.Y. Su, C.F. Li, T. Sun, C. Jiang, Biomimetic dendrimer-peptide conjugates for early multi-target therapy of Alzheimer's disease by inflammatory microenvironment modulation, Adv. Mater. 33 (2021), e2100746.

[57] M.G. Savelieff, G. Nam, J. Kang, H.J. Lee, M. Lee, M.H. Lim, Development of multifunctional molecules as potential therapeutic candidates for Alzheimer's disease, Parkinson's disease, and amyotrophic lateral sclerosis in the last decade, Chem. Rev. 119 (2019) 1221–1322.

[58] J. Rostami, T. Mothes, M. Kolahdouzan, O. Eriksson, M. Moslem, J. Bergstrom, M. Ingelsson, P. O'Callaghan, L.M. Healy, A. Falk, A. Erlandsson, Crosstalk between astrocytes and microglia results in increased degradation of alpha-synuclein and amyloid-beta aggregates, J. Neuroinflammation 18 (2021) 124.

[59] A.B. Lopez-Rodriguez, E. Hennessy, C.L. Murray, A. Nazmi, H.J. Delaney, D. Healy, S.G. Fagan, M. Rooney, E. Stewart, A. Lewis, N. de Barra, P. Scarry, L. Riggs-Miller, D. Boche, M.O. Cunningham, C. Cunningham, Acute systemic inflammation exacerbates neuroinflammation in Alzheimer's disease: IL-1 beta drives amplified responses in primed astrocytes and neuronal network dysfunction, Alzheimer's Dement. 17 (2021) 1735.

[60] C.S. Subhramanyam, C. Wang, Q.D. Hu, S.T. Dheen, Microglia-mediated neuroinflammation in neurodegenerative diseases, Semin. Cell Dev. Biol. 94 (2019) 112–120.

[61] G.M. Tannahill, A.M. Curtis, J. Adamik, E.M. Palsson-McDermott, A.F. McGettrick, G. Goel, C. Frezza, N.J. Bernard, B. Kelly, N.H. Foley, L. Zheng, A. Gardet, Z. Tong, S.S. Jany, S.C. Corr, M. Haneklaus, B.E. Caffrey, K. Pierce, S. Walmsley, F. C. Beasley, E. Cummins, V. Nizet, M. Whyte, C.T. Taylor, H. Lin, S.L. Masters, E. Gottlieb, V.P. Kelly, C. Clish, P.E. Auron, R.J. Xavier, L.A.J. O'Neill, Succinate is an inflammatory signal that induces IL-1 beta through HIF-1 alpha, Nature 496 (2013) 238–242.

[62] D.A. Hume, The many alternative faces of macrophage activation, Front. Immunol. 6 (2015) 370.

[63] D.M. Mosser, The many faces of macrophage activation, J. Leukoc. Biol. 73 (2003) 209–212.

[64] P.J. Crack, J.M. Taylor, U. Ali, A. Mansell, P.J. Hertzog, Potential contribution of NF-kappa B in neuronal cell death in the glutathione peroxidase-1 knockout mouse in response to ischemia-reperfusion injury, Stroke 37 (2006) 1533–1538.

[65] S. Udomruk, B. Wudtiwai, T.H. Shwe, T. Phitak, P. Pothacharoen, M. Phimphilai, P. Kongtawelert, Sesamin suppresses advanced glycation end products induced microglial reactivity using BV2 microglial cell line as a model, Brain Res. Bull. 172 (2021) 190–202.

[66] X.Y. Sun, L.J. Li, Q.X. Dong, J. Zhu, Y.R. Huang, S.J. Hou, X.L. Yu, R.T. Liu, Rutin prevents tau pathology and neuroinflammation in a mouse model of Alzheimer's disease, J. Neuroinflammation 18 (2021) 131.

[67] F. Collin, C. Cheignon, C. Hureau, Oxidative stress as a biomarker for Alzheimer's disease, Biomarkers Med. 12 (2018) 201–203.

[68] B. Halliwell, Reactive oxygen species and the central-nervous-system, J. Neurochem. 59 (1992) 1609–1623.

[69] A.C. Le Lamer, H. Authier, I. Rouaud, A. Coste, J. Boustie, B. Pipy, N. Gouault, Protolichesterinic acid derivatives: alpha-Methylene-gamma-lactones as potent dual activators of PPAR gamma and Nrf2 transcriptional factors, Bioorg. Med. Chem. Lett 24 (2014) 3819–3822.

[70] J.T. Fischedick, M. Standiford, D.A. Johnson, R.C.H. De Vos, S. Todorovic, T. Banjanac, R. Verpoorte, J.A. Johnson, Activation of antioxidant response element in mouse primary cortical cultures with sesquiterpene lactones isolated from *Tanacetum parthenium*, Planta Med. 78 (2012) 1725–1730.

[71] N. Ballatori, S.M. Krance, S. Notenboom, S.J. Shi, K. Tieu, C.L. Hammond, Glutathione dysregulation and the etiology and progression of human diseases, Biol. Chem. 390 (2009) 191–214.
[72] A. Ghantous, H. Gali-Muhtasib, H. Vuorela, N.A. Saliba, N. Darwiche, What made sesquiterpene lactones reach cancer clinical trials? Drug Discov. Today 15 (2010) 668–678.
[73] R.E. Becker, N.H. Greig, E. Giacobini, Why do so many drugs for Alzheimer's disease fail in development? Time for new methods and new practices? J. Alzheimers Dis. 15 (2008) 303–325.
[74] T. Vogels, A.N. Murgoci, T. Hromadka, Intersection of pathological tau and microglia at the synapse, Acta Neuropathol. Commun. 7 (2019) 109.
[75] A. Ittner, L.M. Ittner, Dendritic Tau in Alzheimer's disease, Neuron 99 (2018) 13–27.
[76] L.M. Ittner, Y.D. Ke, F. Delerue, M.A. Bi, A. Gladbach, J. van Eersel, H. Wolfing, B. C. Chieng, M.J. Christie, I.A. Napier, A. Eckert, M. Staufenbiel, E. Hardeman, J. Gotz, Dendritic function of Tau mediates amyloid-beta toxicity in Alzheimer's disease mouse models, Cell 142 (2010) 387–397.
[77] B. Dejanovic, M.A. Huntley, A. De Maziere, W.J. Meilandt, T. Wu, K. Srinivasan, Z. Y. Jiang, V. Gandham, B.A. Friedman, H. Ngu, O. Foreman, R.A.D. Carano, B. Chih, J. Klumperman, C. Bakalarski, J.E. Hanson, M. Sheng, Changes in the synaptic proteome in Tauopathy and rescue of Tau-induced synapse loss by C1q antibodies, Neuron 100 (2018) 1322–1336.e7.
[78] L.H. Lu, Y.T. Mak, M.R. Fang, D.T. Yew, The difference in gliosis induced by beta-amyloid and Tau treatments in astrocyte cultures derived from senescence accelerated and normal mouse strains, Biogerontology 10 (2009) 695–710.
[79] M. Giera, H. Lingeman, W.M.A. Niessen, Recent advancements in the LC- and GC-based analysis of malondialdehyde (MDA): a brief overview, Chromatographia 75 (2012) 433–440.
[80] Y.D. Huang, L. Mucke, Alzheimer mechanisms and therapeutic strategies, Cell 148 (2012) 1204–1222.
[81] P. Sharma, P. Srivastava, A. Seth, P.N. Tripathi, A.G. Banerjee, S.K. Shrivastava, Comprehensive review of mechanisms of pathogenesis involved in Alzheimer's disease and potential therapeutic strategies, Prog. Neurobiol. 174 (2019) 53–89.
[82] A. Khan, T.J. Park, M. Ikram, S. Ahmad, R. Ahmad, M.G. Jo, M.O. Kim, Antioxidative and anti-inflammatory effects of Kojic acid in A beta-induced mouse model of Alzheimer's disease, Mol. Neurobiol. 58 (2021) 5127–5140.
[83] S. Zameer, M. Alam, S. Hussain, D. Vohora, J. Ali, A. Najmi, M. Akhtar, Neuroprotective role of alendronate against APP processing and neuroinflammation in mice fed a high fat diet, Brain Res. Bull. 161 (2020) 197–212.
[84] M.L. Bennett, A.N. Viaene, What are activated and reactive glia and what is their role in neurodegeneration? Neurobiol. Dis. 148 (2021) 105172.
[85] S. Robel, B. Berninger, M. Gotz, The stem cell potential of glia: lessons from reactive gliosis, Nat. Rev. Neurosci. 12 (2011) 88–104.
[86] H.N. Mai, L.T.T. Nguyen, E.J. Shin, D.J. Kim, J.H. Jeong, Y.H. Chung, X.G. Lei, N. Sharma, C.G. Jang, T. Nabeshima, H.C. Kim, Astrocytic mobilization of glutathione peroxidase-1 contributes to the protective potential against cocaine kindling behaviors in mice via activation of JAK2/STAT3 signaling, Free Radic. Biol. Med. 131 (2019) 408–431.
[87] L. Blaszczyk, M. Maitre, T. Leste-Lasserre, S. Clark, D. Cota, S.H.R. Oliet, V. S. Fenelon, Sequential alteration of microglia and astrocytes in the rat thalamus following spinal nerve ligation, J. Neuroinflammation 15 (2018) 349.
[88] S. Jinno, F. Fleischer, S. Eckel, V. Schmidt, T. Kosaka, Spatial arrangement of microglia in hippocampus: a stereological study with astrocytes, Glia 55 (2007) 1334–1347.
[89] T. Ma, E. Klann, Amyloid beta: linking synaptic plasticity failure to memory disruption in Alzheimer's disease, J. Neurochem. 120 (Suppl 1) (2012) 140–148.
[90] T. Hoshino, T. Namba, M. Takehara, N. Murao, T. Matsushima, Y. Sugimoto, S. Narumiya, T. Suzuki, T. Mizushima, Improvement of cognitive function in Alzheimer's disease model mice by genetic and pharmacological inhibition of the EP4 receptor, J. Neurochem. 120 (2012) 795–805.
[91] I. Merfort, Perspectives on sesquiterpene lactones in inflammation and cancer, Curr. Drug Targets 12 (2011) 1560–1573.